

MODIFIED-ENTROPY MODELS FOR THE INTRACLUSTER MEDIUM

G. MARK VOIT¹, GREG L. BRYAN², MICHAEL L. BALOGH³, RICHARD G. BOWER³
ApJ, received 26 February 2002, accepted 15 May 2002

ABSTRACT

We present a set of cluster models that link the present-day properties of clusters to the processes that govern galaxy formation. These models treat the entropy distribution of the intracluster medium as its most fundamental property. Because convection strives to establish an entropy gradient that rises with radius, the observable properties of a relaxed cluster depend entirely on its dark-matter potential and the entropy distribution of its uncondensed gas. Guided by simulations, we compute the intracluster entropy distribution that arises in the absence of radiative cooling and supernova heating by assuming that the gas-density distribution would be identical to that of the dark matter. The lowest-entropy gas would then fall below a critical entropy threshold at which the cooling time equals a Hubble time. Radiative cooling and whatever feedback is associated with it must modify the entropy of that low-entropy gas, changing the overall entropy distribution function and thereby altering the observable properties of the cluster. Using some phenomenological prescriptions for entropy modification based on the existence of this cooling threshold, we construct a remarkably realistic set of cluster models. The surface-brightness profiles, mass-temperature relation, and luminosity-temperature relation of observed clusters all naturally emerge from these models. By introducing a single adjustable parameter related to the amount of intracluster gas that can cool within a Hubble time, we can also reproduce the observed temperature gradients of clusters and the deviations of cooling-flow clusters from the standard luminosity-temperature relation.

Subject headings: cosmology: theory — galaxies: clusters: general — galaxies: evolution — intergalactic medium — X-rays: galaxies: clusters

1. INTRODUCTION

The hot gas in clusters of galaxies seems like it should be easy to understand. Because of the relatively low ratio of baryons to dark matter, the potential well of a cluster should be dark-matter dominated. The dynamical time within a cluster potential is shorter than a Hubble time, so most clusters should be relaxed. Also, the cooling time of the vast majority of intracluster gas is longer than a Hubble time. It would appear that cluster structure ought to be scale-free, as long as the shape of a cluster's potential well does not depend systematically on its mass. If that were the case, then the global properties of clusters, such as halo mass, luminosity-weighted temperature, and X-ray luminosity, would scale self-similarly (Kaiser 1986). In particular, the gas temperature would scale with cluster mass as $T \propto M^{2/3}$ and the bolometric X-ray luminosity would scale with temperature as $L \propto T^2$ in the bremsstrahlung-dominated regime above ~ 2 keV. Indeed, numerical simulations that include gas dynamics but exclude non-gravitational processes such as radiative cooling and supernova heating produce clusters that obey these scaling laws (e.g., Evrard, Metzler, & Navarro 1996; Bryan & Norman 1998; Thomas et al. 2001b).

Real clusters are not so simple. We have known for a decade that the observed luminosity-temperature relation is closer to $L \propto T^3$ (e.g., Edge & Stewart 1991), indicating that non-gravitational processes must influence the density structure of a cluster's core, where most of the luminosity is generated (Kaiser 1991; Evrard & Henry 1991;

Navarro, Frenk & White 1995; Bryan & Norman 1998). The mass-temperature relation, on the other hand, seemed like it ought to be more fundamental and less sensitive to non-gravitational effects. Yet, observations collected over the last few years indicate that this relation also disagrees with both the scale-free predictions and simulations that exclude non-gravitational processes (Horner, Mushotzky, & Scharf 1999; Nevalainen, Markevitch, & Forman 2000; Finoguenov, Reiprich, & Böhringer 2001; Xu, Jin, & Wu 2001). These results derive mostly from resolved X-ray and temperature profiles coupled with the assumption of hydrostatic equilibrium, but they do seem consistent with gravitational lensing measurements (Allen, Schmidt, & Fabian 2001).

Understanding the scaling properties of clusters is of broad importance because these scaling laws are integral to determination of cosmological parameters. For example, the number density of clusters in the local universe reflects the amplitude of matter perturbations on ~ 20 Mpc scales (e.g., Henry & Arnaud 1991; White, Efstathiou, & Frenk 1993; Viana & Liddle 1996; Eke, Cole & Frenk 1996; Kitayama & Suto 1997; Oukbir & Blanchard 1997; Henry 2000). In order to measure this amplitude, one needs accurately measured cluster masses. Gravitational lensing measurements of cluster mass have grown rapidly in sophistication during the last few years, but X-ray determined cluster temperatures, converted to cluster masses using the mass-temperature relation, remain the most commonly used mass measurement for cosmological studies. Thus, any inaccuracies in the mass-temperature

¹ Space Telescope Science Institute, 3700 San Martin Drive, Baltimore, MD 21218, voit@stsci.edu

² Physics Department, University of Oxford, Keble Road, Oxford OX1 3RH, UK, gbryan@astro.ox.ac.uk

³ Department of Physics, University of Durham, South Road, Durham DH1 3LE, UK, M.L.Balogh@durham.ac.uk, R.G.Bower@durham.ac.uk

relation propagate into uncertainties in cosmological parameters derived from clusters (e.g., Voit 2000). A number of authors have recently re-evaluated the perturbation amplitude implied by cluster observations using a variety of techniques that circumvent the standard mass-temperature relation (Reiprich & Böhringer 2001; Van Waerbeke et al. 2001; Seljak 2002; Viana, Nichol, & Liddle 2002). The results are disconcertingly different from those based on the standard relation, generally implying a much lower power-spectrum amplitude. Clearly a better understanding of clusters is needed, and ideally, we would like to know how the present-day properties of clusters are linked to the physics of galaxy formation.

The physical processes most likely to break the expected self-similarity of clusters are heating by supernovae or active galactic nuclei and radiative cooling, although other possibilities such as magnetic pressure or cosmic-ray pressure have not been ruled out. A large number of studies have investigated how the structure of the intracluster medium changes when these processes are included. Because treating all of these processes in sufficient detail is extremely complicated, various approximations have been employed. These include numerical simulations that administer a particular amount of energy input at early times or adopt some other phenomenological prescription for injecting energy (e.g., Metzler & Evrard 1994; Navarro, Frenk, & White 1995; Metzler & Evrard 1997; Bialek, Evrard, & Mohr 2001; Borgani et al. 2001a; da Silva et al. 2001; Bryan & Voit 2001), analytical models for spherically symmetric accretion of preheated gas (e.g., Cavaliere, Menci & Tozzi 1999; Tozzi & Norman 2001), and semi-analytic models that consider the merger and star formation history of clusters (e.g., Wu, Fabian, & Nulsen 1998, 2000; Balogh, Babul, & Patton 1999; Bower et al. 2001; Babul, Balogh, Lewis, & Poole 2002). Most of these papers have focused on heating of the gas, but recent work has also examined the possibility that radiative cooling is primarily responsible (e.g., Knight & Ponman 1997; Sugihara & Ostriker 1998; Pearce et al. 2000; Bryan 2000; Muanwong et al. 2001; Thomas et al. 2001a; Lewis et al. 2001). Two broad conclusions emerge from such studies: (1) radiative cooling without feedback probably locks too high a fraction of baryons into condensed objects, and (2) if heating is uniformly distributed, the amount required to produce realistic clusters is quite large, probably exceeding ~ 1 keV per baryon. Introducing this much energy through supernova heating strains the bounds of plausibility, given how many metals are observed in the intracluster medium (e.g., Balogh, Babul, & Patton 1999; Valageas & Silk 1999; Kravtsov & Yepes 2000; Bower et al. 2000; although see Loewenstein 2000).

Here, we revisit an approach pioneered by Bower (1997), focusing on entropy as the most fundamental characteristic of the intracluster medium. Analyzing clusters in terms of entropy has two advantages. The first is that convection within clusters acts as an entropy-sorting device, shuttling low-entropy material to the cluster core and high-entropy material to the cluster's outskirts. Convective stability is achieved when specific entropy becomes a monotonically increasing function of radius. Thus, if we can determine the entropy distribution of the gas in a cluster and we know the structure of its dark-matter

halo, we can predict the structure of that cluster in its relaxed state. In the idealized cases that we will consider, we will assume that clusters are spherically symmetric, dark-matter dominated, in hydrostatic equilibrium, and in convective equilibrium. The second advantageous property of entropy is that, in the absence of non-gravitational processes, the entropy distribution of a cluster can be readily computed using either hydrodynamical simulations or spherically symmetric analytical models. Then, the effects of non-gravitational heating and radiative cooling can be implemented as modifications of that entropy distribution.

In Voit & Bryan (2001), we introduced a simple scheme for computing cluster models, taking advantage of these properties of the intracluster entropy distribution to show how heating and cooling conspire to produce a cluster L - T relation quite similar to what is observed. This paper explores those modified-entropy models in more detail, showing that the observable properties of these model clusters are quite similar to those of real clusters on many counts. Section 2 describes how we construct those models and analyzes how cluster properties depend on both halo concentration and entropy modification. Section 3 uses relations between halo mass and halo concentration to define sets of cluster models determined entirely by the underlying cosmology. We then compare the model clusters with observations of the surface-brightness profiles of clusters, the temperature gradients of clusters, the mass-temperature relation, and the luminosity-temperature relation. In every case, our models reproduce the observations, with little need for adjustable parameters. In section 4, we explore how the present-day intracluster entropy distribution emerges from hierarchical cosmological models. Section 5 summarizes our conclusions.

2. MODIFIED ENTROPY MODELS

In this section we develop a family of modified-entropy models of clusters based on two parameters, one specifying the concentration of the cluster's dark-matter halo and the other specifying the entropy level at which cooling and feedback modify the intracluster entropy distribution. We begin by casting the equilibrium equations in dimensionless form and selecting appropriate boundary conditions. Then we assume that the unmodified entropy distribution determined by gravitational processes alone would produce a gas density distribution similar to the dark-matter density distribution. Because the innermost gas in such a cluster can cool in much less than a Hubble time, we proceed to investigate several potential modifications of the entropy distribution by radiative cooling and subsequent feedback. In each case, we show how both entropy modification and the shape of the underlying dark-matter halo affect the surface-brightness profile of a cluster, its luminosity-weighted temperature, its temperature gradient, and its X-ray luminosity. Two important results emerge from this analysis: (1) the temperature of a cluster of a given mass is determined primarily by halo concentration and is affected only modestly by entropy modification, and (2) altering the intracluster entropy distribution at the scale set by radiative cooling leads to an L_X - T relation that has the observed slope at $z = 0$ and that evolves very little with time.

2.1. Equilibrium Structure

The equilibrium structure of the intracluster medium is determined by three things, the gravitational potential of the cluster's dark matter, the entropy distribution of the cluster's gas, and the confining pressure at the outer boundary of the cluster. In order to solve for that structure, one must integrate the equations of hydrostatic equilibrium and gas mass conservation,

$$\frac{dP}{dr} = -\frac{GM(<r)}{r^2}\rho \quad (1)$$

$$\frac{dM_g}{dr} = 4\pi r^2 \rho \quad , \quad (2)$$

using the equation of state $P = K\rho^\gamma$, where γ is the adiabatic index and K specifies the adiabat of the gas. In this system of equations, $M(<r)$ is the total mass within radius r , M_g is the gas mass within that radius, and the other symbols have their usual meanings. Throughout this paper, we will assume that the gas mass is gravitationally negligible and that $\gamma = 5/3$, as appropriate for an ideal monatomic gas.

In a sufficiently relaxed cluster, convection ensures that $K(r)$ monotonically increases with radius. Thus, if one knows $M_g(K)$, the entropy distribution of the intracluster medium expressed in terms of the mass of gas with $P\rho^{-5/3} < K$, then one can use the inverse relation $K(M_g)$ to solve the equilibrium equations that determine the cluster's structure. Because this crucial quantity K is so closely related to specific entropy, we will often refer to it as the ‘‘entropy’’ of the gas, even though the standard thermodynamic entropy per particle for an ideal monatomic gas is $s = \ln K^{3/2} + \text{const.}$

2.1.1. Dimensionless Form

We can gain insight into the key parameters that control the structure of the intracluster medium by investigating a family of dimensionless models for clusters in hydrostatic and convective equilibrium. Because the virial radius of a cluster lies close to the radius r_{200} within which the mean matter density of the cluster is 200 times the critical density ρ_{cr} , we elect to represent radii in terms of $\hat{r} \equiv r/r_{200}$ and gas density in terms of $\hat{\rho} \equiv \rho/f_b\rho_{200}$, where $\rho_{200} = 200\rho_{cr}$ and $f_b = 0.02/\Omega_m h^2$ is the fractional contribution of baryons to the total mass of the universe. One can then rewrite the equilibrium equations in dimensionless form as follows:

$$\frac{d\hat{P}}{d\hat{r}} = -2\frac{\hat{M}}{\hat{r}^2}\hat{\rho} \quad (3)$$

$$\frac{d\hat{f}_g}{d\hat{r}} = 3\hat{r}^2\hat{\rho} \quad , \quad (4)$$

where $M_{200} = (4\pi/3)r_{200}^3\rho_{200}$ is the virial mass, $T_{200} = GM_{200}\mu m_p/2r_{200}$ is the temperature in energy units¹ of the corresponding singular isothermal sphere, $\hat{P} = P/[T_{200}f_b\rho_{200}(\mu m_p)^{-1}]$ is the dimensionless pressure, $\hat{M} = M(<r)/M_{200}$ is the dimensionless mass within \hat{r} , and $\hat{f}_g = M_g/(f_b M_{200})$ is the fraction of a cluster's baryons in the intracluster medium within radius \hat{r} . The corresponding dimensionless entropy distribution is $\hat{K}(\hat{f}_g) = K/[T_{200}(f_b\rho_{200})^{-2/3}(\mu m_p)^{-1}]$, and we will also make use of the quantity $\hat{T} = P\rho^{-1}\mu m_p T_{200}^{-1}$.

¹ Boltzmann's constant k is absorbed into T throughout the paper.

General solutions to these equations can be found for a few idealized cases. For example, if the potential is a singular isothermal sphere and the gas is also isothermal, then we have $\hat{P} \propto \hat{\rho} \propto \hat{r}^{-2}$, $f_g \propto \hat{r}$, and $\hat{K} \propto \hat{r}^{4/3}$ for a monatomic ideal gas. If instead the mass profile follows the form of Navarro, Frenk & White (1997; NFW hereafter), with $\hat{M} \propto [\ln(1+c\hat{r}) - c\hat{r}(1+c\hat{r})^{-1}]$ where c is the concentration parameter, then the equation of hydrostatic equilibrium becomes (see Wu, Fabian, & Nulsen 2000)

$$\frac{d\hat{P}}{d\hat{r}} = 2\hat{\rho} \left[\ln(1+c) - \frac{c}{1+c} \right]^{-1} \frac{d}{d\hat{r}} \left[\frac{\ln(1+c\hat{r})}{\hat{r}} \right] \quad . \quad (5)$$

Given an isentropic gas in which $\hat{P}\hat{\rho}^{-5/3} = \hat{K} = \text{const.}$ we thus obtain $\hat{\rho} \propto [\hat{r}^{-1} \ln(1+c\hat{r}) + C]^{3/2}$, where C is a constant of integration.

2.1.2. Boundary Conditions

A particular solution to the equilibrium equations can be found by choosing \hat{P} and \hat{f}_g at the origin and integrating outwards. The gas mass fraction at the origin is always zero by definition, but there is some freedom in the choice of $\hat{P}_0 \equiv \hat{P}(0)$. Any given choice of \hat{P}_0 corresponds to a unique ICM structure with a unique luminosity and temperature profile, but which solutions are the physical ones?

Here is where the confining pressure comes into play. It is generally assumed that accreting matter confines the ICM in the neighborhood of r_{200} . The pressure at r_{200} would then be determined by the ram pressure of the infalling matter. Now suppose that $K(M_g)$ has been modified by non-gravitational processes. For example, heating might drive gas out of the cluster potential, pushing the accretion shock to a radius beyond r_{200} . Alternatively, cooling and condensation might reduce the total gas mass of the intracluster medium so that the accretion shock moves inward. In either case the radius at which the integration of hydrostatic equilibrium should terminate differs from r_{200} .

So what is the termination radius r_{max} at which $f_g f_b M_{200}$ equals the total uncondensed gas mass, and what is the pressure at that radius? In a freely falling accretion flow with a constant mass flux, the density should vary as $v_{ff}^{-1} r^{-2}$, where $v_{ff} \propto \hat{r}^{-1/2} \sqrt{\ln(1+c\hat{r})}$ is the free-fall velocity from $\hat{r} \gg 1$ in an NFW potential. We therefore assume that the accretion pressure scales with radius as $\hat{P}_{acc}(\hat{r}) \propto \hat{r}^{-5/2} \sqrt{\ln(1+c\hat{r})}$, and we normalize that pressure to equal the unmodified NFW value (see § 2.2) at $\hat{r} = 1$. Various choices of \hat{P}_0 will lead to pressure profiles that intersect $\hat{P}_{acc}(\hat{r})$ at different values of \hat{r}_{max} , each corresponding to a unique value of $f_g(\hat{r}_{max})$ determined by a particular integration. The correct solution is the one that gives the proper value for the uncondensed gas mass at the radius where the gas pressure equals the accretion pressure.

In practice, the physically reasonable solutions are not particularly sensitive to the outer boundary condition. In the models that follow, applying the boundary condition $\hat{P} = \hat{P}_{acc}$ at $\hat{r} = 1$ would lead to similar results. However, the value of f_g derived at $\hat{r} = 1$ using this boundary

condition is not physically significant and can even be inconsistent with models in which cooling and condensation significantly reduce the maximum value of f_g . One example of a physically *unreasonable* boundary condition is requiring $f_g = 1$ at $\hat{r} = 1$. Such a requirement does not allow intracluster gas to expand beyond r_{200} even when heating substantially raises the intracluster entropy. In the limit of extreme heating, this condition therefore artificially boosts the central pressure, density, and temperature, leading to an unphysically large cluster luminosity.

2.1.3. Integrated Characteristics

Once a correct solution has been identified, one can compute two quantities that correspond to the dimensionless luminosity and luminosity-weighted temperature:

$$\hat{L} = 3 \int_0^{\hat{r}^{max}} \hat{\rho}^2 \hat{r}^2 d\hat{r} \quad (6)$$

$$\hat{T}_{lum} = 3\hat{L}^{-1} \int_0^{\hat{r}^{max}} \hat{T} \hat{\rho}^2 \hat{r}^2 d\hat{r} \quad (7)$$

As long as the cooling function $\Lambda(T)$ remains sufficiently constant within the gas contributing the bulk of the luminosity, the actual luminosity-weighted temperature is $T_{lum} \approx T_{200} \hat{T}_{lum}$, and the bolometric X-ray luminosity is

$$L \approx \frac{4\pi}{3} r_{200}^3 \left(\frac{n_p}{n_e} \right) \bar{n}_e^2 \Lambda(T_{lum}) \hat{L} \quad (8)$$

where $\bar{n}_e = (n_e/\rho) f_b \rho_{200} = 1.2 \times 10^{-4} (\Omega_M/0.33)^{-1} \text{cm}^{-3}$. Scaling to a 10 keV cluster at $z = 0$ gives

$$L \approx (9.0 \times 10^{43} h^{-3} \text{erg s}^{-1}) \left(\frac{T_{200}}{10 \text{ keV}} \right)^{3/2} \left(\frac{\Omega_M}{0.33} \right)^{-2} \times \Lambda_{23}(T_{lum}) \hat{L} \quad (9)$$

where $\Lambda_{23}(T_{lum}) = \Lambda(T_{lum})/(10^{-23} \text{erg cm}^3 \text{s}^{-1})$.

The emission-measure profile and emissivity-weighted temperature profile are also of interest. Thus, we define the following dimensionless analogs as functions of the projected radius \hat{r}_\perp :

$$\hat{S}(\hat{r}_\perp) = 2 \int_0^{\sqrt{\hat{r}^{max}{}^2 - \hat{r}_\perp^2}} \hat{\rho}^2 d\hat{l} \quad (10)$$

$$\hat{T}_\perp(\hat{r}_\perp) = 2\hat{S}^{-1} \int_0^{\sqrt{\hat{r}^{max}{}^2 - \hat{r}_\perp^2}} \hat{T} \hat{\rho}^2 d\hat{l} \quad (11)$$

where $\hat{l} = \sqrt{\hat{r}^2 - \hat{r}_\perp^2}$ is the dimensionless distance along the line of sight.

2.2. Unmodified Solutions

Before exploring the consequences of modifying the entropy of intracluster gas, we need to know what the entropy distribution would be if it were not modified. To simplify matters, we will assume that the underlying dark matter profile of the cluster is of NFW form with some concentration parameter c . This parameter typically ranges from $c \sim 5$ for hot clusters to $c \sim 10$ for groups of galaxies (see § 3.1). If the intracluster medium were collisionless, then its density profile would be identical to that of the dark matter. Thus, we define the unmodified entropy distribution $\hat{K}_0(M_g)$ of a cluster of concentration c to be that of gas in hydrostatic equilibrium in the cluster potential with a density profile identical to that of the dark matter.

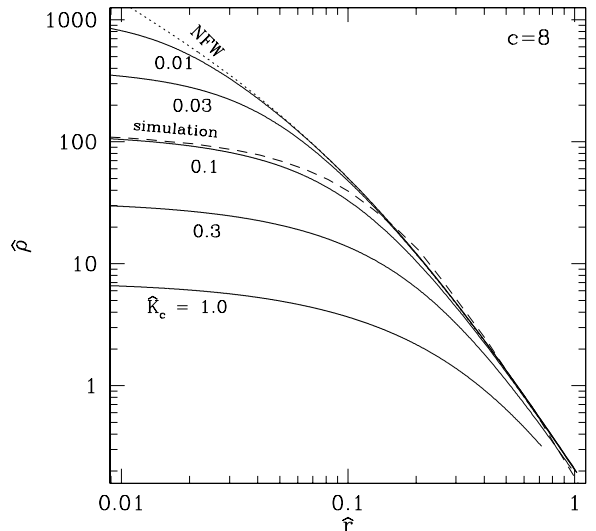


FIG. 1.— Intracluster density profiles in dimensionless units. The dotted line shows the matter density ($\hat{\rho}$) of an NFW profile of concentration $c = 8$ in units of the mean density within r_{200} as a function of radius (\hat{r}) in units of r_{200} . The dashed line shows the density profile of a simulated cluster whose dark matter halo is well approximated by an NFW halo with $c = 8$. Outside of $\hat{r} = 0.1$, these curves closely correspond. The solid lines show how the run of density with radius changes as the entropy distribution of an unmodified $c = 8$ NFW halo is truncated at progressively larger values of the dimensionless entropy \hat{K}_c . For these cases, $\hat{\rho}$ is the gas density in units of the mean density of the unmodified gas. Notice that the model with $\hat{K}_c = 0.1$ is quite similar to the gas density distribution from the simulation.

Numerical experiments reveal that the entropy distribution of intracluster gas in clusters simulated without radiative cooling or supernova heating is quite similar to the NFW form throughout most of the cluster but is elevated above NFW within the cluster’s core. Figure 1 shows the density distribution of a cluster simulated with an adaptive-mesh refinement code (Norman & Bryan 1998; Bryan 1999) for the Santa Barbara cluster comparison project (Frenk et al. 1999). The dotted line labeled “NFW” shows an NFW density distribution with $c = 8$, which is very close to the underlying dark-matter distribution of the cluster. The dashed line labeled “simulation” shows the gas-density distribution from that same simulation. Agreement is quite close outside 10% of the virial radius, but the gas density levels off within that radius, implying that the lowest-entropy gas has a somewhat higher entropy than assumed in our unmodified distribution K_0 . However, this discrepancy at the low-entropy end of the distribution is inconsequential to the modified-entropy models that follow because the entropy of the discrepant gas will always be subject to further modification.

The unmodified distribution is also somewhat discrepant with simulations at the high-entropy end. Assuming hydrostatic equilibrium and an NFW gas-density law near the virial radius leads to gas temperatures that are 20-30% higher than those in our fiducial simulation. Thus, our unmodified entropy levels at large radii are slightly higher than what a numerical simulation would produce. However, in order to properly reproduce the density profile near the virial radius in a hydrostatic model, we must retain these elevated entropy levels. This overestimate at the cluster’s outskirts has virtually no effect on emissivity-weighted global quantities, such as L and T_{lum} , but if one

is interested in the temperature of cluster gas near r_{200} , then departures from hydrostatic equilibrium, which are outside the scope of our models, must be taken into account.

2.3. Entropy Modification

Modification of this baseline entropy distribution is inevitable because clusters simulated without radiative cooling are physically inconsistent. In general, the gas at the center of such a simulated cluster can radiate many times its thermal energy within a Hubble time, resulting in cluster luminosities that vastly exceed those observed (e.g., Muanwong et al. 2001; Bryan & Voit 2001). Condensation and removal of the lowest-entropy gas from the intracluster medium must happen at some level, because that is how the cluster's galaxies form stars. Furthermore, the most massive of these stars must explode, resulting in supernova feedback. Condensed gas accreting onto an active galactic nucleus can provide additional feedback (Heinz, Reynolds, & Begelman 1998; Kaiser & Alexander 1999; Quilis, Bower, & Balogh 2001; Reynolds, Heinz, & Begelman 2002; Böhringer et al. 2002). All of these processes will modify the entropy distribution of the intracluster medium, but modeling them in detail is a daunting task.

Because the physics of feedback is so complex, we shall adopt a highly simplistic phenomenological approach to entropy modification. Instead of trying to model all the consequences of heating and cooling we will restrict our investigation to three qualitatively different modifications of the entropy distribution K_0 : (1) truncation of the distribution, (2) shifting of the distribution, and (3) radiative losses from the distribution. Each of these modifications depends on a single entropy threshold parameter K_c , which we take to be the entropy at which the cooling time of gas of temperature T_{200} equals the age of the universe. Thus, for each type of entropy modification, we obtain a two-parameter family of modified-entropy models specified by a concentration c and a dimensionless entropy \hat{K}_c .

As in Voit & Bryan (2001), we use an approximate cooling function for gas with a metallicity of one-third solar to determine the appropriate entropy threshold. According to this approximation, the threshold for cooling within 15 Gyr can be expressed as

$$K_c \approx \frac{135 \text{ keV cm}^2}{\mu m_p} \left(\frac{\rho}{n_e} \right)^{-2/3} \left(\frac{T_{\text{lum}}}{2 \text{ keV}} \right)^\zeta, \quad (12)$$

with $\zeta = 2/3$ for $T > 2 \text{ keV}$ and $\zeta = 0$ for $T < 2 \text{ keV}$. Converting this threshold to dimensionless units yields

$$\hat{K}_c \approx 0.164 \hat{T}_{\text{lum}} \left(\frac{T_{\text{lum}}}{2 \text{ keV}} \right)^{\zeta-1} \left(\frac{\Omega_M}{0.33} \right)^{-2/3}. \quad (13)$$

As long as $\hat{T}_{\text{lum}} \approx 1$ (see § 2.5), then $\hat{K}_c \approx 0.1$ will be appropriate for the hottest clusters ($\sim 10 \text{ keV}$) and $\hat{K}_c \approx 0.5 - 1.0$ will be appropriate for the coolest ($\sim 0.5 \text{ keV}$) groups.

2.3.1. Truncation

One simple yet physically motivated way to modify the entropy distribution of intracluster gas is to truncate it at \hat{K}_c (Bryan 2000; Voit & Bryan 2001). Mathematically, we

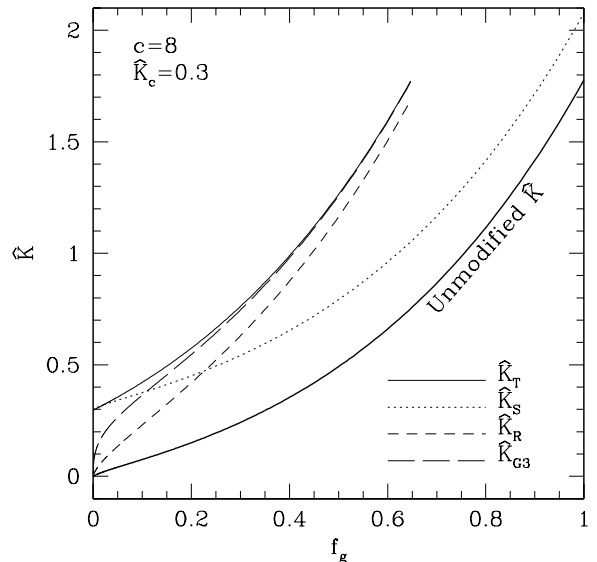


FIG. 2.— Modified entropy distributions. The thick solid line shows how dimensionless entropy \hat{K} rises with f_g , the fraction of a cluster's baryons in the intracluster medium within radius \hat{r} , for an unmodified $c = 8$ NFW halo. Gas in the unmodified halo is assumed to be in hydrostatic equilibrium with a density profile identical to that of the dark matter. The thin solid line illustrates the entropy distribution $\hat{K}_T(f_g)$ that results when the unmodified distribution is truncated at $\hat{K}_c = 0.3$, corresponding to a horizontal translation of the unmodified distribution. The dotted line shows $\hat{K}_S(f_g)$, the unmodified distribution shifted vertically by $\hat{K}_c = 0.3$. The long- and short-dashed lines show two different modifications designed to mimic radiative losses from the unmodified distribution (see § 2.3.3). These lines correspond to a reduction of \hat{K} at each point of the unmodified distribution, followed by a horizontal translation so that $\hat{K}(0) = 0$.

define the truncated distribution to be

$$\hat{K}_T(f_g) \equiv \hat{K}_0(f_g + f_c), \quad (14)$$

where f_c is defined by $\hat{K}_0(f_c) = \hat{K}_c$. Such a modification corresponds to removing all the gas with a cooling time less than a Hubble time and ignoring the effects of cooling on the rest of the intracluster medium. This type of modification can be viewed either as an extreme form of cooling, in which all the gas below the critical threshold condenses, or an extreme form of heating, in which all the gas below the threshold is heated to very high entropy ($\hat{K} \gg 1$) and convects beyond the virial radius of the cluster. Figure 1 shows some gas density profiles resulting from different values of \hat{K}_c . The thin solid line labeled \hat{K}_T in Figure 2 shows the truncated entropy distribution for $c = 8$ and $\hat{K}_c = 0.3$.

Notice that the maximum value of f_g in these truncated models is less than unity because some of the gas has been removed from the intracluster medium. The thick solid line in Figure 3 illustrates how the fraction $f_{g,max} = 1 - f_c$ of a cluster's baryons that remain in the intracluster medium depends on \hat{K}_c . For hot clusters this fraction is $\sim 90\%$, but for cool groups it drops below 50% . Nevertheless, the outer radius \hat{r}_{max} of the intracluster gas remains close to r_{200} , even when $f_{g,max}$ drops below 0.5 . Figure 1 shows the reason. As the entropy threshold for truncation rises, the central entropy of the cluster also rises. The resulting density profile is therefore much flatter for large values of \hat{K} , enabling a smaller amount of gas

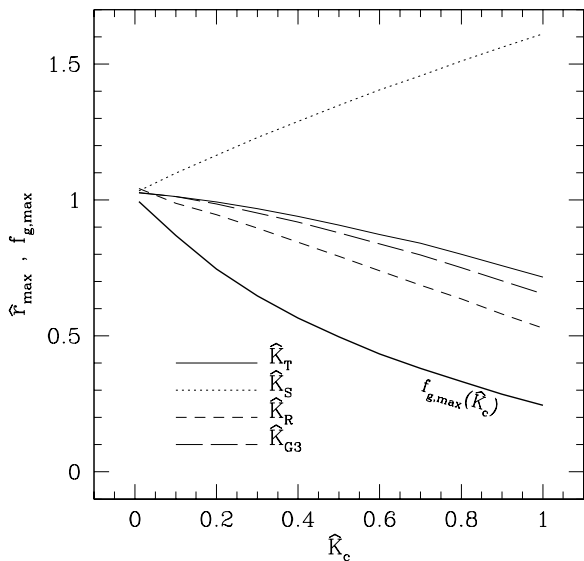


FIG. 3.— Maximum radius and baryon content of the intracluster medium in modified-entropy models. The thick solid line shows how $f_{g,\max}$, the fraction of a cluster’s baryons residing in the intracluster medium, depends on the entropy threshold \hat{K}_c in the modified distributions \hat{K}_T , \hat{K}_R , and \hat{K}_{G3} . The other lines show how \hat{r}_{\max} , the maximum radius of the intracluster medium, depends on \hat{K}_c in each of these modified distributions.

to fill a similar volume. Note also that the density profile of a modified-entropy model with $c = 8$ and $\hat{K}_c = 0.1$ is quite similar to that of a $c = 8$ cluster simulated without cooling and feedback, suggesting that the cooling threshold may have only a modest effect on the structure of the hottest clusters.

2.3.2. Shift

Another way to modify intracluster entropy is to add a constant term \hat{K}_c to the unmodified entropy distribution (Voit & Bryan 2001). This type of modification is a convenient way to mimic “preheated” models for cluster formation that inject a fixed amount of entropy per particle into the intergalactic medium at some early time. In this case, the modified entropy distribution is defined by

$$\hat{K}_S(f_g) \equiv \hat{K}_0(f_g) + \hat{K}_c. \quad (15)$$

The dotted line in Figure 2 shows this distribution for $c = 8$ and $\hat{K}_c = 0.3$. Because entropy has been added but no gas has been removed, the outer radius for models with a shifted entropy distribution extends beyond the usual virial radius (see Figure 3). Qualitatively, this corresponds to heating that inflates the intracluster medium, driving the accretion shock to larger radii.

Comparing the structure of shifted models to truncated models reveals interesting similarities. Figure 4 depicts the dimensionless density profiles for $\hat{K}_c = 0.1, 0.3$, and 1.0 in clusters with $c = 8$. The run of density with radius is virtually identical for the shifted and truncated models when $\hat{K}_c = 0.1$ and is still quite similar when $\hat{K}_c = 0.3$. Thus, for most of the interesting range of entropy thresholds, there is little observable difference between shifted models and truncated models. However, as \hat{K}_c rises to 1.0 , the density profile of the shifted model becomes noticeably flatter than that of the truncated model.

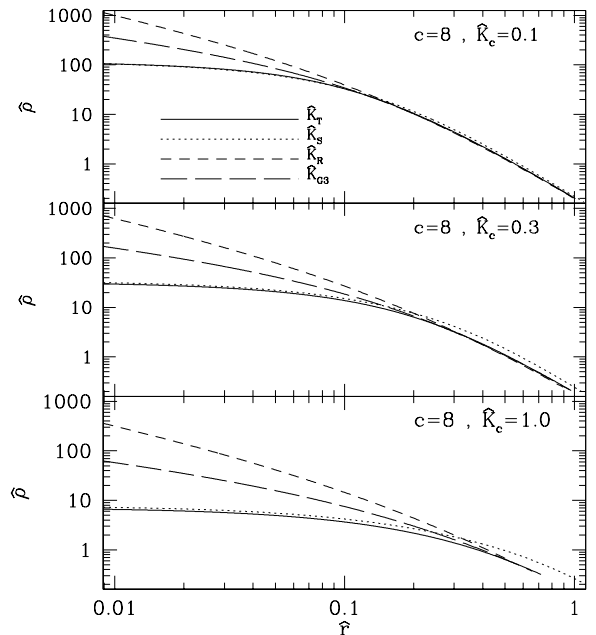


FIG. 4.— Density profiles for modified entropy models with $c = 8$ and $\hat{K}_c = 0.1, 0.3$, and 1.0 . Solid lines show $\hat{\rho}(\hat{r})$ for truncated models (\hat{K}_T), dotted lines represent shifted models (\hat{K}_S), and the long- and short-dashed lines represent two types of radiative-loss model (\hat{K}_R and \hat{K}_{G3}). The density structure of truncated and shifted models is almost indistinguishable for small values of \hat{K}_c . The radiative-loss models have the elevated central densities characteristic of cooling-flow clusters.

Similarity between the truncated and shifted models at the lower entropy thresholds arises because the unmodified entropy \hat{K}_0 depends approximately linearly on f_g for small \hat{K} . Thus, shifting the distribution by \hat{K}_c and truncating it at \hat{K}_c both produce similar modified entropy distributions and therefore similar density, temperature, and pressure distributions in the inner regions of the cluster. That is why entropy modification by heating and cooling can have similar effects on the luminosity and temperature of clusters as long as they establish similar values of the minimum entropy.

2.3.3. Radiative Losses

Observations show that many clusters contain gas with a cooling time less than a Hubble time (Fabian 1994), motivating us to consider slightly more complicated modifications to the entropy distribution. Radiative cooling reduces the the specific entropy of a gas parcel according to

$$\frac{ds}{dt} = \frac{d \ln K^{3/2}}{dt} = -\frac{\mu m_p n_p n_e \Lambda(T)}{\rho T}. \quad (16)$$

This entropy equation can be rewritten to eliminate the dependence on gas density:

$$\frac{dK^{3/2}}{dt} = -\left(\frac{n_p n_e}{\rho^2}\right) (\mu m_p)^{-1/2} T^{1/2} \Lambda(T). \quad (17)$$

In general, the rate at which entropy declines will depend on the prevailing hydrodynamic conditions, standard examples being isobaric cooling or isochoric cooling.

However, for the purposes of this toy model, let us assume that the right-hand side of this equation remains constant. We make this rather arbitrary assumption for two physical reasons. First, within the temperature range $0.1 \text{ keV} \lesssim T \lesssim 2 \text{ keV}$, the quantity $T^{1/2}\Lambda(T)$ is approximately constant. Second, as gas settles within a nearly isothermal potential, work done by compression will attempt to maintain the temperature of that gas near the characteristic temperature of the halo. Thus, we are motivated to use the following modification to represent radiative losses:

$$\hat{K}_R(f_g) \equiv \{[\hat{K}_0(f_g + f_c)]^{3/2} - \hat{K}_c^{3/2}\}^{2/3}. \quad (18)$$

This modification corresponds to reducing the value of $\hat{K}^{3/2}$ by the constant amount $\hat{K}_c^{3/2}$ throughout the entropy distribution and discarding all the gas with $\hat{K} < 0$. The short-dashed line in Figure 2 shows an example of the resulting distribution for $c = 8$ and $\hat{K}_c = 0.3$, and a similar line in Figure 3 shows how the maximum radius depends on \hat{K}_c .

It will also be interesting to investigate a generalization of this radiative-loss model:

$$\hat{K}_{G\alpha}(f_g) \equiv \{[\hat{K}_0(f_g + f_c)]^\alpha - \hat{K}_c^\alpha\}^{1/\alpha}, \quad (19)$$

in which the tunable parameter α enables us to adjust the amount of gas below the cooling threshold. In the limit $\alpha \rightarrow \infty$, this generalized distribution becomes identical to the truncated distribution. In what follows, we will focus on the intermediate case of $\alpha = 3$, represented by the symbol \hat{K}_{G3} and long-dashed lines in the relevant figures.

Figure 4 compares the density distributions that result from the radiative-loss models with the truncated and shifted models. For $\hat{K}_c = 0.1$, all the density profiles are very similar at $\hat{r} > 0.1$, because the entropy profiles are nearly identical there. However, within that radius, entropy in the radiative-loss models drops below \hat{K}_c , allowing for considerably greater compression and higher central density. This trend becomes more pronounced at higher \hat{K}_c because the proportion of the intracluster medium below the cooling threshold is even larger.

2.4. Entropy Modification and Surface Brightness

Modified-entropy models generated through shifts and truncations of the unmodified entropy distribution produce surface-brightness profiles that are strikingly similar to the β -model profiles of many real clusters, at least within about 30% of the virial radius. Figure 5 shows the dimensionless emission measure \hat{S} as a function of projected radius \hat{r} for three different truncated models, each with $c = 8$. As the threshold entropy progresses from $\hat{K}_c = 0.1$, characteristic of clusters, through $\hat{K}_c = 0.3$ to $\hat{K}_c = 1.0$, characteristic of groups, the $\hat{S}(\hat{r}_\perp)$ profile substantially flattens. As long as $\Lambda(T)$ does not change dramatically with radius, these emission-measure profiles will be nearly identical to the surface-brightness profiles.

For comparison, Figure 5 also shows some β -model profiles selected to match the modified-entropy models. These β -model profiles are defined by $\hat{S} \propto [1 + (r/r_c)^2]^{-3\beta+1/2}$, where r_c is the core radius and β determines the asymptotic slope (Cavaliere & Fusco-Femiano 1978). In each case, the β -model closely tracks the modified-entropy model within $0.3r_{200}$. Beyond that radius, the emission

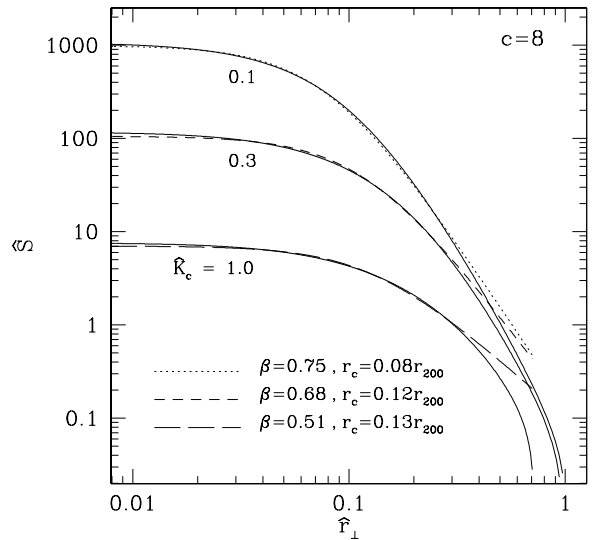


FIG. 5.— Dimensionless emission measure \hat{S} as a function of projected radius \hat{r}_\perp . The solid lines show $\hat{S}(\hat{r})$ for three modified entropy models with $c = 8$, truncated at $\hat{K}_c = 0.1, 0.3$, and 1.0 . The dotted and dashed lines show emission measure profiles derived from β -models with $\hat{S} \propto [1 + (r/r_c)^2]^{-3\beta+0.5}$. Notice that the β -models are very good approximations to the modified-entropy models within $0.3r_{200}$.

measures of the β -models exceed those of the modified-entropy models, but owing to the low surface brightness at large radii, the β -model parameters of clusters and groups have generally been measured within $0.3 - 0.5r_{200}$. Recent measurements by Vikhlinin, Forman, & Jones (1999) suggest that cluster surface brightness does indeed fall below the best fitting β -model near the virial radius.

In order to determine how the best-fitting β and r_c depend on c and \hat{K}_c , we performed surface-brightness weighted fits over a grid of modified entropy models. Because the best-fit parameters depend somewhat on the portion of the profile being fitted, we elected to do these fits over two different radial intervals: $0.03 < \hat{r}_\perp < 0.3$ and $0.05 < \hat{r}_\perp < 1.0$. Results for truncated (\hat{K}_T) models are shown in Figure 6, and those for shifted (\hat{K}_S) models are shown in Figure 7. Because the profiles in the shifted models tend to be shallower, the corresponding β values are somewhat smaller, particularly for low values of \hat{K}_c . However, in both cases, the best-fitting β values span the observed range for clusters and groups of galaxies (see § 3.2.1).

2.5. Entropy Modification and Cluster Temperature

One consequence of raising the core entropy of a cluster is a boost in the luminosity-weighted temperature of the intracluster gas. Figure 8 shows that increasing \hat{K}_c raises the temperature of gas at all radii in both the shifted and truncated models. Amplification of the central temperature can be quite extreme, exceeding $3T_{200}$ when \hat{K}_c rises to 1.0 . However, the resulting enhancement of the luminosity-weighted temperature is not nearly as dramatic. The value of \hat{T}_{lum} turns out to depend more critically on the concentration parameter c than on the entropy threshold, as demonstrated in Figure 9.

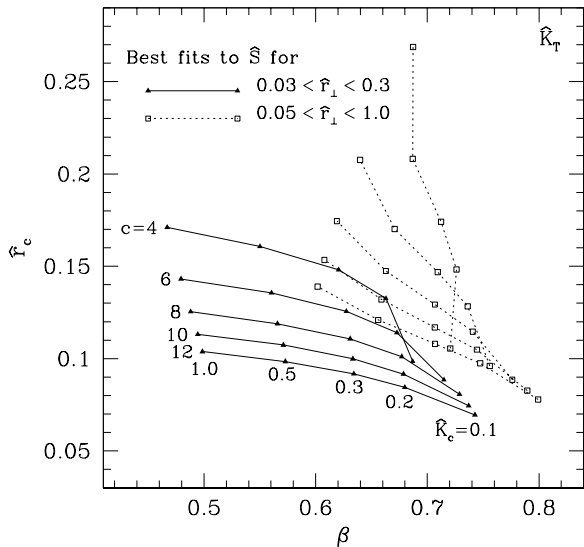


FIG. 6.— Best-fitting β -model parameters for truncated modified-entropy models. Each line gives the best-fitting (β, r_c) pair for a particular value of the concentration c . The points on each line show best fits for five different values of the entropy threshold. The progression $\hat{K}_c = 1.0, 0.5, 0.3, 0.2, 0.1$ runs from the upper left to lower right in each case. Because the best fits depend somewhat on the fitted interval, we depict best fits over the interval $0.03 < \hat{r}_\perp < 0.3$ with solid triangles and solid lines and best fits over the interval $0.05 < \hat{r}_\perp < 1.0$ with empty squares and dotted lines.

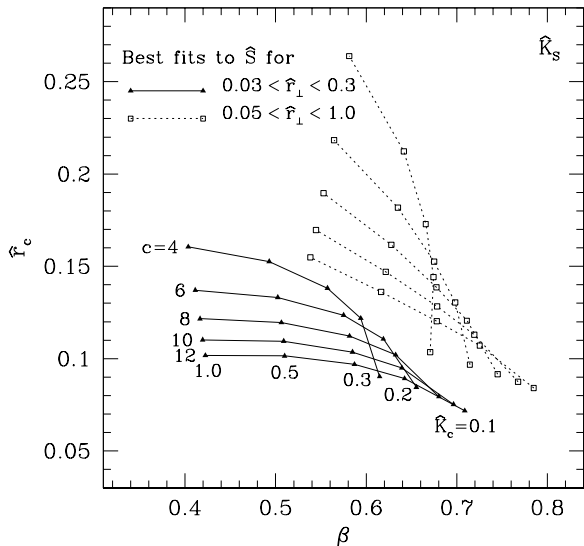


FIG. 7.— Best-fitting β -model parameters for shifted modified-entropy models. Each line gives the best-fitting (β, r_c) pair for a particular value of the concentration c . The points on each line show best fits for five different values of the entropy threshold. The progression $\hat{K}_c = 1.0, 0.5, 0.3, 0.2, 0.1$ runs from the upper left to lower right in each case. Because the best fits depend somewhat on the fitted interval, we depict best fits over the interval $0.03 < \hat{r}_\perp < 0.3$ with solid triangles and solid lines and best fits over the interval $0.05 < \hat{r}_\perp < 1.0$ with empty squares and dotted lines.

The reason that raising the core entropy of gas in an NFW potential has only a modest effect on its luminosity-weighted temperature involves both the gas density profile

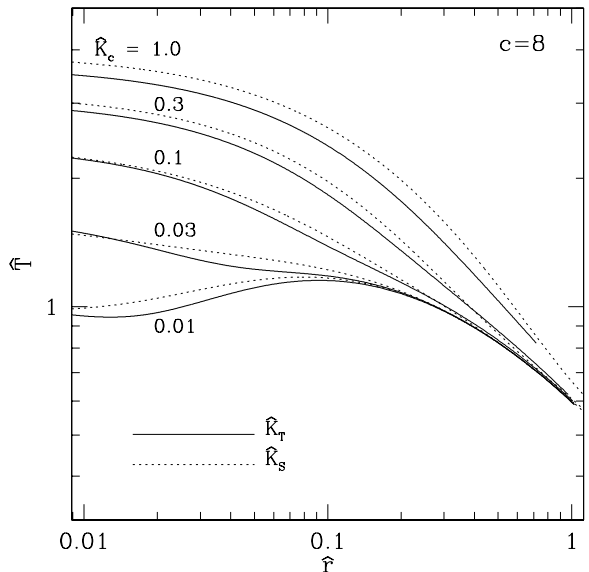


FIG. 8.— Dimensionless temperature profiles. Solid lines show how temperature (\hat{T}) depends on radius (\hat{r}) in models with truncated entropy distributions (\hat{K}_T). Dotted lines show how temperature depends on radius in models with shifted entropy distributions (\hat{K}_S). Raising the entropy threshold \hat{K}_c increases the temperature at all radii for both kinds of entropy modification. This increase is slightly larger for shifted models because the extra gas at large radii leads to slightly higher central pressures.

and the dark-matter density profile. Extra entropy flattens the density profile of intracluster gas, diminishing the relative luminosity of gas in the core. The characteristic radius of gas contributing the bulk of the cluster's luminosity therefore moves outward. Because the shape of an NFW halo is steeper than isothermal at $\hat{r} > 1/c$, the characteristic temperature of gas within such a halo declines outside that radius (see Figure 8). Thus, the rise in gas temperature resulting from an increase in \hat{K}_c is largely offset by an increased contribution to the total luminosity from lower-temperature gas at larger radii. This effect is most pronounced in the shifted models, which have substantial amounts of relatively cool gas beyond $\hat{r} = 1$. In those models, \hat{T}_{lum} actually *declines* as \hat{K}_c approaches unity.

The large central temperatures in the shifted and truncated cases also seem somewhat unrealistic in light of observations showing either level or radially increasing temperature gradients within cluster cores (e.g., Arnaud et al. 2001a,b; Allen et al. 2001). In order to compare these temperatures more directly with observations, we must look at \hat{T}_\perp , the luminosity-weighted temperature along various lines of sight through a cluster. Figure 10 illustrates how \hat{T}_\perp depends on projected radius \hat{r}_\perp in clusters with $c = 8$, $\hat{K}_c = 0.3$, and four different kinds of entropy modification. Projected temperatures at $\hat{r}_\perp < 0.1$ in both the shifted and truncated models are still quite high ($\hat{T}_\perp \approx 2T_{200}$). However, the core temperatures in the radiative-loss models look more like those in real clusters (see § 3.2.2), rising with radius in the innermost regions and peaking between $1.2T_{200}$ and $1.6T_{200}$ at $\sim 0.05r_{200}$ in these particular models.

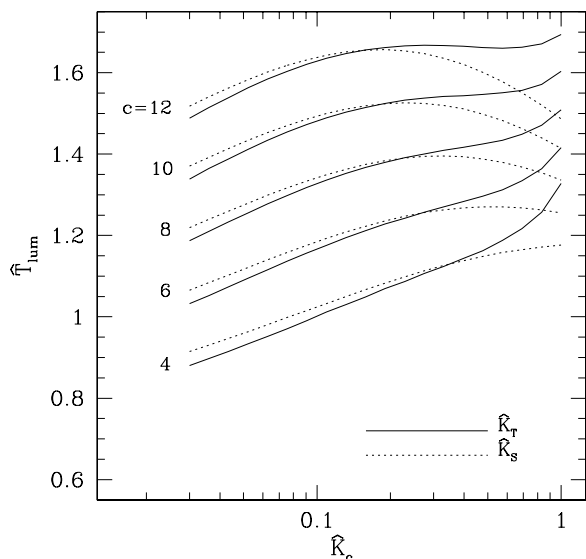


FIG. 9.— Dimensionless luminosity-weighted temperatures (\hat{T}_{lum}) as a function of entropy threshold (\hat{K}_c) for halos of concentration $c = 4, 6, 8, 10,$ and 12 . Solid lines depict truncated models (\hat{K}_T); dotted lines depict shifted models (\hat{K}_S). The dependence of \hat{T}_{lum} on \hat{K}_c is rather modest over the interesting range $0.1 < \hat{K}_c < 1.0$, especially for larger values of c . This effect arises because a larger proportion of the emission from high- \hat{K}_c clusters comes from $\hat{r} > 1/c$, where temperatures are lower than in the core. This outward shift of surface brightness largely offsets the rise in temperature at all radii evident in Figure 8.

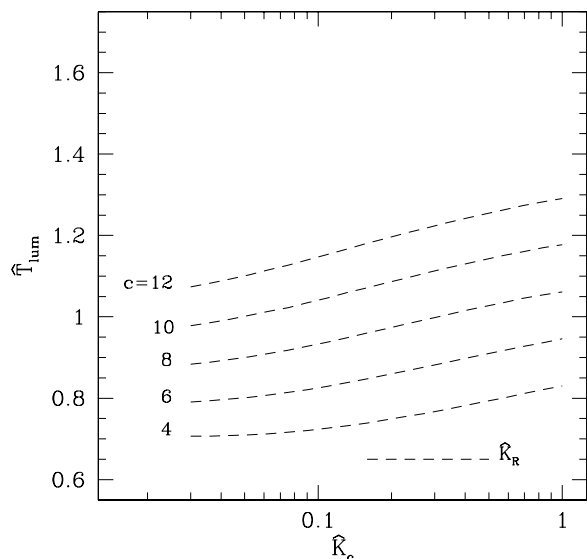


FIG. 11.— Dimensionless luminosity-weighted temperatures for the standard radiative-loss model (\hat{K}_R). Comparison of these $\hat{T}_{\text{lum}}(\hat{K}_c)$ relations with those in Figure 9 shows that emission from the core gas lowers the luminosity-weighted temperature by $\sim 30\%$, relative to the shifted and truncated models.

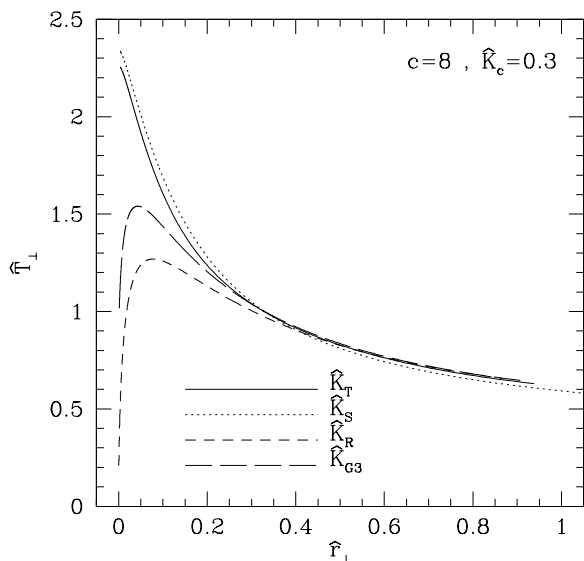


FIG. 10.— Dimensionless luminosity-weighted line-of-sight temperature \hat{T}_{\perp} as a function of projected radius \hat{r}_{\perp} . The solid and dotted lines representing truncated and shifted models, respectively, both begin at rather high temperature ($\approx 2T_{200}$) at small radii and proceed to decline monotonically with radius. The long- and short-dashed lines representing radiative-loss models (see § 2.3.3) begin at low temperature at $\hat{r} = 0$ and rise to a maximum at $\approx 0.05r_{200}$, in better accord with observed clusters (see § 3.2.2).

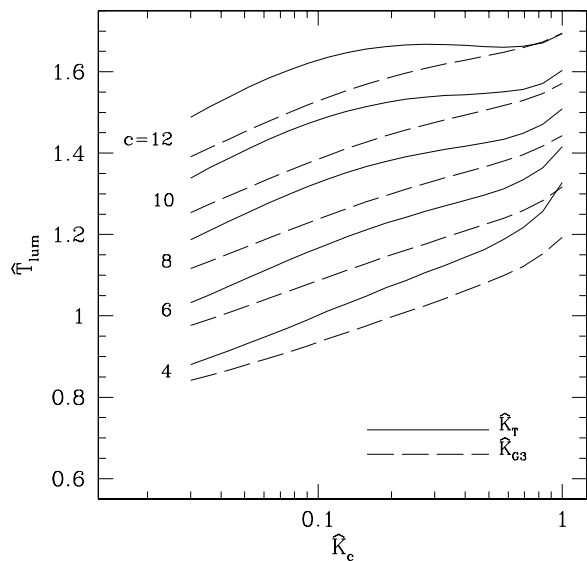


FIG. 12.— Dimensionless luminosity-weighted temperatures for generalized radiative-loss model \hat{K}_{G3} with $\alpha = 3$. Solid lines show the $\hat{T}_{\text{lum}}(\hat{K}_c)$ relations for truncated models, and long-dashed lines show the corresponding relations for the radiative-loss models. Luminosity-weighted temperature is $\sim 10\%$ smaller in these generalized radiative-loss models. The difference is less dramatic than in the $\alpha = 3/2$ case because the amount of gas below \hat{K}_c is smaller, resulting in somewhat higher core temperature and somewhat lower core density and luminosity.

Cool gas in the cores of clusters with entropy modified through radiative losses can significantly affect the luminosity-weighted temperature if the fraction of gas below \hat{K}_c is relatively large. Figure 11 shows that \hat{T}_{lum} for a given concentration c and entropy threshold \hat{K}_c is $\sim 30\%$ lower in the standard radiative-loss model (\hat{K}_R) than in the corresponding truncated model. This effect is also present but not nearly so strong in the generalized radiative-loss model with $\alpha = 3$, where \hat{T}_{lum} is $\sim 10\%$ lower than in the truncated models (see Figure 12).

2.6. Entropy Modification and Cluster Luminosity

All of our schemes for entropy modification substantially lower the luminosities of clusters. Figure 13 shows how dimensionless luminosity \hat{L} depends on the entropy threshold \hat{K}_c for clusters with $c = 8$. In all cases, luminosity declines by over an order of magnitude as \hat{K}_c rises from 0.1 to 1. This decline is shallowest for the shifted model because the additional gas at large radii contributes significantly to the total luminosity when $\hat{K}_c \sim 1$. Note also that \hat{L} is over twice as large in the standard radiative-loss case (\hat{K}_R) because a large proportion of the luminosity in such models comes from the dense core. Luminosity enhancement in the $\alpha = 3$ radiative-loss model is more moderate—only a few tens of percent greater than in the truncated case.

Analyzing how \hat{L} depends on \hat{K}_c leads to some important insights into how the cooling threshold determines the luminosity-temperature relation of clusters and groups. Figure 14 shows that $\hat{L} \propto \hat{K}_c^{-3/2}$ is a good approximation to the \hat{L} - \hat{K}_c relation for truncated models in the range $0.1 < \hat{K}_c < 1.0$. This scaling reflects the asymptotic slope of the NFW density profile. Notice that the outer portions of the density profiles in Figure 1 track the underlying NFW profile of the dark matter, and the inner portions are nearly isentropic with $\hat{K} \approx \hat{K}_c$. One can therefore approximate the density profile of a truncated model by joining an isentropic density profile to an NFW profile at the radius \hat{r}_K at which the density of the unmodified NFW profile is $\hat{\rho}_K \sim \hat{K}_c^{-3/2}$. The analytical isentropic solution from § 2.1.1 tells us that $\hat{\rho} \propto [\hat{r}^{-1} \ln(1 + c\hat{r})]^{3/2}$ within \hat{r}_K , so the luminosity from the isentropic gas scales $\propto \hat{\rho}_K^2 \hat{r}_K^3$. The luminosity from the NFW portion of the profile scales in the same way for the radii of interest. Thus, for larger values of \hat{r} , where the density of the NFW profile approaches $\hat{\rho} \propto \hat{r}^{-3}$, we have $\hat{L} \propto \hat{\rho}_K \propto \hat{K}_c^{-3/2}$.

This particular scaling of \hat{L} with \hat{K}_c has some very interesting consequences. Section 2.1.3 showed that the physical luminosity of a cluster scales as $L \propto r_{200}^3 \rho_{cr}^2 \Lambda \hat{L}$. In order to substitute physical quantities for \hat{L} , we need to recognize that $\hat{K}_c^{3/2} \propto K_c^{3/2} T_{200}^{-3/2} \rho_{cr}$ and that $K_c^{3/2} \propto T^{1/2} \Lambda t_H$, where t_H is the age of the universe. We therefore obtain

$$L \propto T_{\text{lum}}^{5/2} \hat{T}_{\text{lum}}^{-3} (H t_H)^{-1} , \quad (20)$$

where H is the Hubble constant at time t_H .

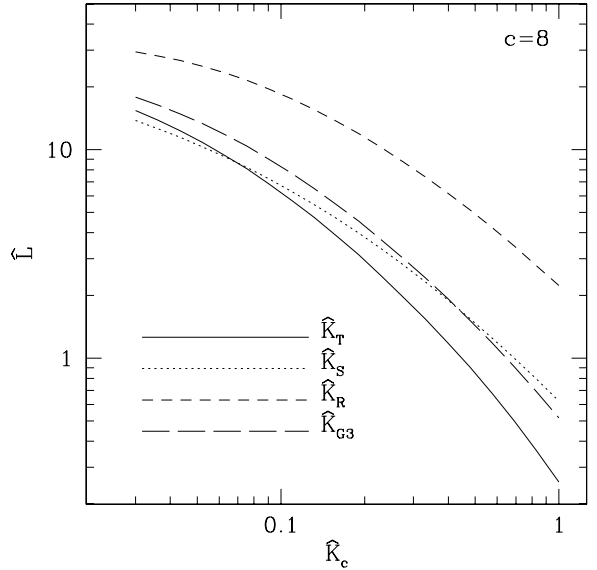


FIG. 13.— Dependence of dimensionless luminosity \hat{L} on the entropy threshold \hat{K}_c for clusters with $c = 8$. The decline of \hat{L} with increasing \hat{K}_c is strong for all types of entropy modification. The effect is stronger in the truncated (\hat{K}_T) and radiative-loss (\hat{K}_R , \hat{K}_{G3}) models than in the shifted model (\hat{K}_S) because the latter has more gas at large radii, which contributes significantly to \hat{L} when the entropy threshold is high.

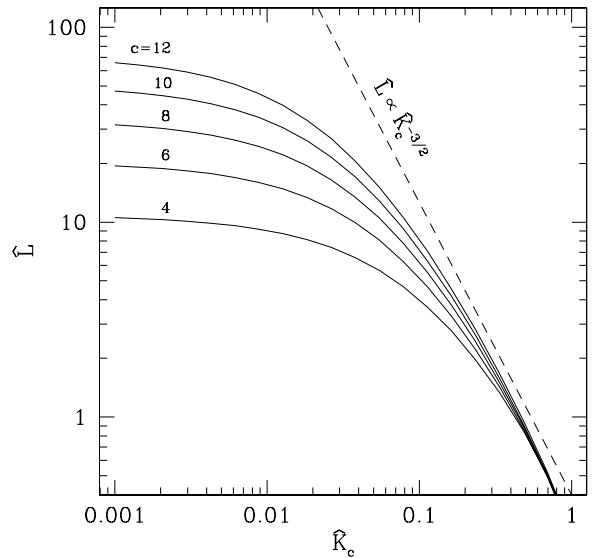


FIG. 14.— Dimensionless luminosity \hat{L} as a function of entropy threshold \hat{K}_c in truncated (\hat{K}_T) models for clusters with concentration $c = 4, 6, 8, 10,$ and 12 . The cluster luminosities in these models sharply decline as \hat{K}_c increases. For $0.1 < \hat{K}_c < 1.0$ this decline approximately scales as $\hat{L} \propto \hat{K}_c^{-3/2}$.

The following three features of this expression are particularly noteworthy:

- The power-law slope it predicts for the X-ray $L \propto T^b$ relation is very close to the observed slope of $b \approx 2.6 - 2.9$ (e.g., Markevitch 1998; Arnaud & Evrard 1999). Because the halos of low-temperature groups have higher concentrations than high-temperature clusters (see § 3.1), we expect \hat{T}_{lum} to decline by a factor ~ 1.3 as T_{lum} rises by an order of magnitude. This dependence on concentration steepens the power-law slope implied by equation (20) to $b \approx 2.8$.
- The L - T relation does not depend on the form of the cooling function, which scales as $\Lambda \propto T^{1/2}$ in the free-free cooling regime at $T > 2$ keV and as $\Lambda \propto T^{-1/2}$ in the line-cooling regime at $T < 2$ keV. If the entropy threshold in real clusters did not depend on Λ , then we would expect a distinct steepening of the L - T relation as T rises through ~ 2 keV, which is not observed. Equation (20) is independent of Λ because the dimensionless gas mass within \hat{r}_K scales $\propto \hat{\rho}_K \hat{r}_K^3$, and thus remains approximately constant in an NFW halo for $\hat{r}_i > 1/c$. The cooling time of that gas is $\sim t_H$, so its physical luminosity scales $\propto M_{200} T_{200} t_H^{-1}$. This scaling law also applies to the entire cluster, because the luminosity of gas outside \hat{r}_K scales in lockstep with gas inside \hat{r}_K . Applying the relation $M_{200} \propto T_{200}^{3/2} H^{-1}$ thus leads back to equation (20), except for the \hat{T}_{lum} factor.
- Finally, the L - T relation implied by equation (20) changes very little with time, again in agreement with observations (Mushotzky & Scharf 1997; Donahue et al. 1999; Della Ceca et al. 2000; Borgani et al. 2001b). That happens because the mass of a cluster of a given temperature declines $\propto H^{-1}$ with increasing redshift. According to the $L \propto M_{200} T_{200} t_H^{-1}$ scaling, the resulting decline in the intracluster gas mass compensates almost precisely for the drop in the cooling threshold owing to the shorter cooling time t_H .

This scaling breaks down at the low-temperature end, where $\hat{K}_c \gtrsim 1$, because the entire intracluster (or intragroup) medium in the truncated and shifted cases becomes effectively isentropic. Then, the gas density determined by the cooling threshold is $\propto T/\Delta t_H$, and the luminosity from within r_{200} scales as $L \propto T_{\text{lum}}^{7/2} \Lambda^{-2} \hat{T}_{\text{lum}}^{-3/2} (H t_H)^{-2} H^{-1}$. Thus, we should expect the L - T relation for low-temperature halos to be steeper than for clusters, roughly $L \propto T^{4.5}$ for $\Lambda \propto T^{-1/2}$, and we should expect the luminosity of objects at a given temperature to increase with time.

In order to make further progress, we will need to understand how halo concentration depends on halo mass.

3. MODELING REAL CLUSTERS

The previous section explored the properties of dimensionless modified-entropy models for clusters depending

on two parameters, the halo concentration parameter c and an entropy-threshold parameter \hat{K}_c . As in Voit & Bryan (2001), we argued that the crucial entropy threshold should be the entropy level at which intracluster gas would cool in a Hubble time. Now we will use a set of relations between halo concentration and halo mass to construct modified-entropy models for real clusters. In these models, the halo mass M_{200} determines the concentration parameter c . The mass and halo concentration then set the temperature of the cluster, and this temperature sets the level of the entropy threshold K_c . Cluster properties are therefore determined primarily by the overall cosmological model, because it fixes the global baryon fraction, the relation between halo mass and concentration, and the Hubble time that governs $K_c(T)$. Some of a cluster's properties, such as the temperature of the innermost gas, also depend on the chosen scheme for entropy modification. The properties of the resulting modified-entropy models turn out to be remarkably similar to those of observed clusters and groups.

The section begins by defining the M_{200} - c relations we will use and comparing them to some of the scarce data. Then, we explore the structure of the intracluster medium in our modified-entropy cluster models, showing that the observed relationship between β and T_{lum} may be more than just a selection effect and demonstrating how entropy modification can lead to temperature profiles similar to those observed in both the inner and outer regions of clusters. We go on to compare the mass-temperature relation from our modified-entropy models to observations, showing that the models reproduce the observational results of Nevalainen et al. (2000) and Finoguenov et al. (2001). We also compare the L_X - T_{lum} relation from our models to cluster data, again showing excellent agreement. Much of the dispersion of this relation, in both the models and the data, stems from differences in the amount of gas below the cooling threshold, and we conclude with some speculations about what governs these differences.

3.1. Concentration Parameter

The concentration of a dark matter halo is determined by its formation history. Early formation generally leads to a denser core and thus a higher concentration. Low-mass halos, which tend to collapse earlier in time, are therefore expected to be somewhat more concentrated than high-mass halos. Because a halo's collapse and merger history determines its concentration, the relation between concentration and halo mass depends on the underlying cosmological model, specified by the matter density Ω_M , the dark-energy density Ω_Λ , the normalization σ_8 of the perturbation spectrum, and the shape of that spectrum, often parameterized by Γ (Bardeen et al. 1986; Sugiyama 1995). In this paper, we will restrict our attention to currently-favored Λ CDM models, in which the resulting clusters turn out to be thoroughly consistent with observations.

Several versions of the concentration parameter c_Δ can be found in the literature, each defined with respect to a radius r_Δ within which the mean halo density is $\Delta \rho_{cr}$. Here we will define c with respect to r_{200} , in order to be consistent with the models developed in the previous section; thus, $c \equiv c_{200}$. Figure 15 shows various relations between halo mass and c_{200} that can be found in the lit-

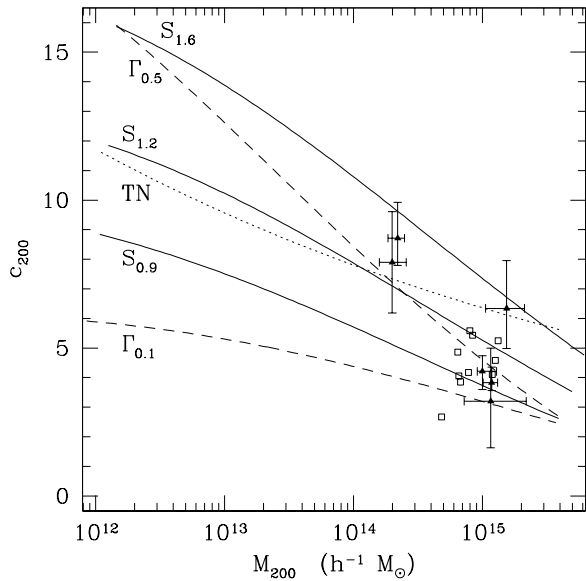


FIG. 15.— Concentration parameter (c_{200}) as a function of halo mass (M_{200}). Solid triangles give concentrations derived from *Chandra* observations of real clusters by Allen et al. (2001). Empty squares give the concentrations of clusters simulated by Eke, Navarro, & Frenk (1998) in a Λ CDM cosmology with $\sigma_8 = 1.1$. Solid lines show c_{200} values predicted by models $S_{0.9}$, $S_{1.2}$, and $S_{1.6}$ from Eke et al. (2001), for a Λ CDM cosmology in which $\sigma_8 = 0.9, 1.2$, and 1.6 , respectively, for a power spectrum with shape parameter $\Gamma = 0.2$. Dashed lines show c_{200} given by models $\Gamma_{0.1}$ and $\Gamma_{0.5}$ from Eke et al. (2001), for which $\Gamma = 0.1$ and 0.5 , respectively, and $\sigma_8 = 0.9$. The dotted line labeled TN shows the c_{200} values from the fit of Tozzi & Norman (2001) to the NFW prescription for a Λ CDM cosmology with $\sigma_8 = 1.1$.

erature. The *Chandra* observations of Allen et al. (2001) suggest that concentrations corresponding to $c_{200} \approx 4 - 6$ are appropriate for massive ($\sim 10^{15} M_\odot$) clusters. Concentrations of groups are less certain because they are more model-dependent, and the dispersion in c_{200} is expected to increase at lower halo masses (Afshordi & Cen 2002).

In this section, we will adopt the halo mass-concentration relations predicted by models $S_{0.9}$ and $S_{1.2}$ from Eke, Navarro, & Steinmetz (2001), which are consistent with the *Chandra* data on massive clusters. Both models are derived from N -body simulations of Λ CDM cosmologies with $\Omega_M = 0.3$, $\Omega_\Lambda = 0.7$, and $h = 0.65$. The power spectrum in each model has a shape parameter $\Gamma = 0.2$, but the normalization of the power spectrum differs: $\sigma_8 = 0.9$ in model $S_{0.9}$ and $\sigma_8 = 1.2$ in model $S_{1.2}$. The higher normalization in model $S_{1.2}$ leads to halos that are about 30% more concentrated. Figure 16 shows the dependence of \hat{K}_c on halo mass that follows from model $S_{1.2}$; the entropy thresholds for model $S_{0.9}$ are very similar.

3.2. Cluster Structure

The cluster models we analyze in this section are completely determined by the assumed relationship between halo mass and concentration (either $S_{0.9}$ or $S_{1.2}$) and the chosen scheme for entropy modification (\hat{K}_T , \hat{K}_S , \hat{K}_R , or \hat{K}_{G3}). For each halo mass, we compute the bolometric X-ray luminosity L_X , luminosity-weighted temperature T_{lum} , X-ray surface-brightness profile $S_X(r_\perp)$, and projected temperature profile $T_\perp(r_\perp)$. Unlike in § 2.1.3, each integral includes a cooling function $\Lambda(T)$ drawn from the

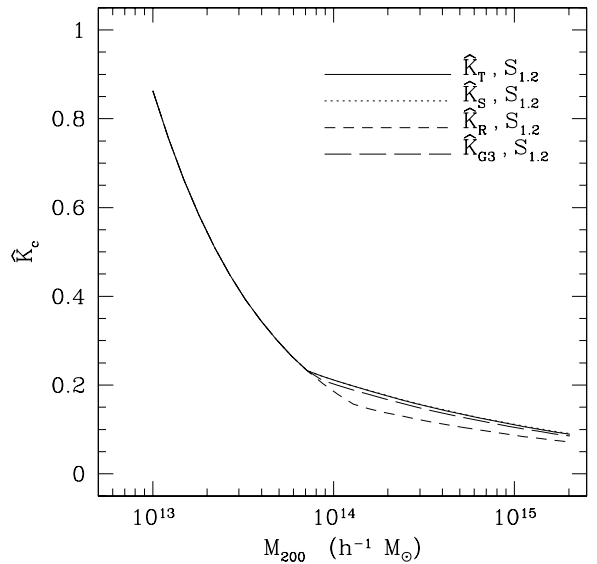


FIG. 16.— Dimensionless entropy threshold (\hat{K}_c) determined by cooling as a function of halo mass M_{200} . The lines show the entropy thresholds for truncated models (solid line), shifted models (dotted line), and radiative-loss models with $\alpha = 3/2$ (short-dashed line), and $\alpha = 3$ (long-dashed line), assuming the halo mass-concentration relation from model $S_{1.2}$. The corresponding thresholds for model $S_{0.9}$ are very similar. Above $10^{14} h^{-1} M_\odot$, different entropy-modification schemes produce slightly different dimensionless thresholds because the temperature T_{lum} associated with a given halo mass is slightly different. Equations (12) and (13) give the entropy threshold K_c and dimensionless entropy threshold \hat{K}_c , respectively, as functions of temperature.

models of Raymond & Smith (1977) for gas with 30% solar metallicity. We will first focus on the spatially resolved properties of these model clusters, showing how their surface-brightness profiles and temperature gradients compare with those of observed clusters.

3.2.1. Surface-Brightness Profiles

Modified-entropy models of groups tend to have flatter surface-brightness profiles than hot clusters, in accordance with observations (e.g., Ponman et al. 1999; Horner et al. 1999). Because the surface-brightness profiles of both real clusters and our modified-entropy models are well described by β -models with $S_X \propto [1 + (r/r_c)^2]^{-3\beta+1/2}$ inside of $0.3r_{200}$ (see § 2.4), we compare our models with the data by comparing the best-fitting β -model parameters. Figure 17 shows how β and r_c depend on T_{lum} in truncated modified-entropy models with relation $S_{1.2}$ and in the cluster data of Finoguenov et al. (2001). The models reproduce the observed range of both parameters and the observed rise in each parameter with increasing temperature. However, the observed dispersion in each parameter at a given temperature is quite large. Wu & Xue (2002) find the same kind of temperature dependence in their cluster models, based on the work of Bryan (2000), which are very similar to the truncated models developed in this paper.

Some of the dispersion in β and r_c at a given temperature may stem from selection effects. Because the surface-brightness profiles of modified-entropy clusters continually steepen with radius, unlike those of β -models, the best-fitting β and r_c depend somewhat on the range of radii being fit. Figure 17 shows that the best-fitting values of β and r_c both decline as the surface-brightness threshold of

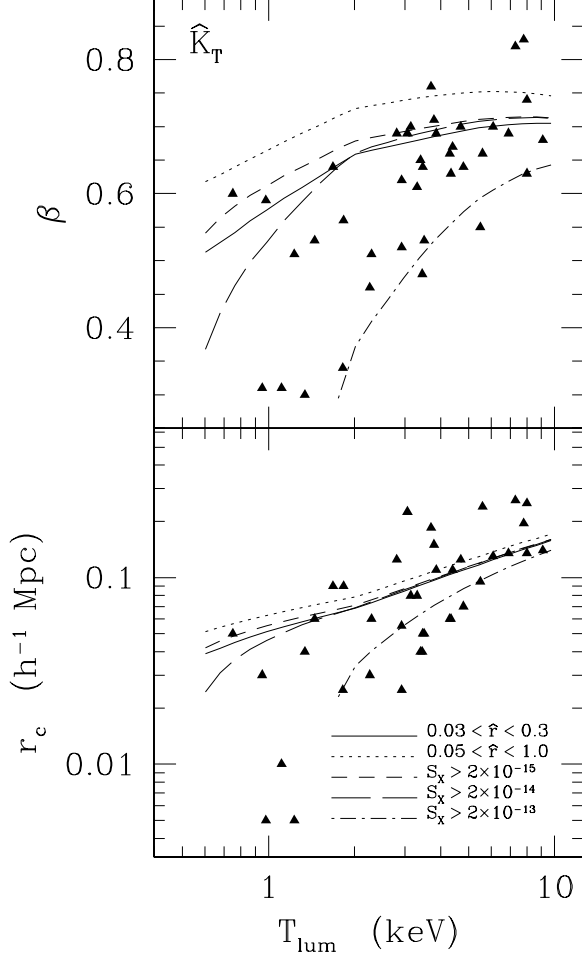


FIG. 17.— Best-fitting β -model parameters as a function of luminosity-weighted temperature T_{lum} . In a β -model, X-ray surface brightness declines with radius as $S_X \propto [1 + (r/r_c)^2]^{-3\beta+1/2}$, where r_c is the core radius and β determines the asymptotic slope. Triangles show measured values of β (upper panel) and r_c (lower panel) compiled by Finoguenov et al. (2001). Solid lines show the values of these parameters in the best fits to truncated modified entropy models (\hat{K}_T) over the radial range $0.03 < \hat{r} < 0.3$, where $\hat{r} \equiv r/r_{200}$. Dotted lines show the best-fitting values over the range $0.05 < \hat{r} < 1.0$. The other lines show best fits above surface-brightness thresholds of $2 \times 10^{-15} \text{ erg cm}^{-2} \text{ s}^{-1} \text{ arcmin}^{-2}$ (short-dashed lines), $2 \times 10^{-14} \text{ erg cm}^{-2} \text{ s}^{-1} \text{ arcmin}^{-2}$ (long-dashed lines), and $2 \times 10^{-13} \text{ erg cm}^{-2} \text{ s}^{-1} \text{ arcmin}^{-2}$ (dot-dashed lines).

the fit rises from $2 \times 10^{-15} \text{ erg cm}^{-2} \text{ s}^{-1} \text{ arcmin}^{-2}$ through $2 \times 10^{-14} \text{ erg cm}^{-2} \text{ s}^{-1} \text{ arcmin}^{-2}$ to $2 \times 10^{-13} \text{ erg cm}^{-2} \text{ s}^{-1} \text{ arcmin}^{-2}$. This effect is more severe for groups than for clusters because their overall surface brightness is smaller. The figure also shows that fits over the radial range $0.05 < r/r_{200} < 1.0$ yield slightly larger β and r_c than fits over $0.03 < r/r_{200} < 0.3$. Komatsu & Seljak (2001) noted a similar surface-brightness selection effect in their polytropic models for clusters. However, the rise of β with T_{lum} in their models is entirely due to this surface-brightness bias. In our models, it is largely a consequence of the greater impact of entropy modification on groups. Puzzlingly, this selection effect becomes stronger at low surface brightness levels in the models of Wu & Xue (2002), perhaps because their boundary condition leads to a less precipitous decline in S_X near the virial radius.

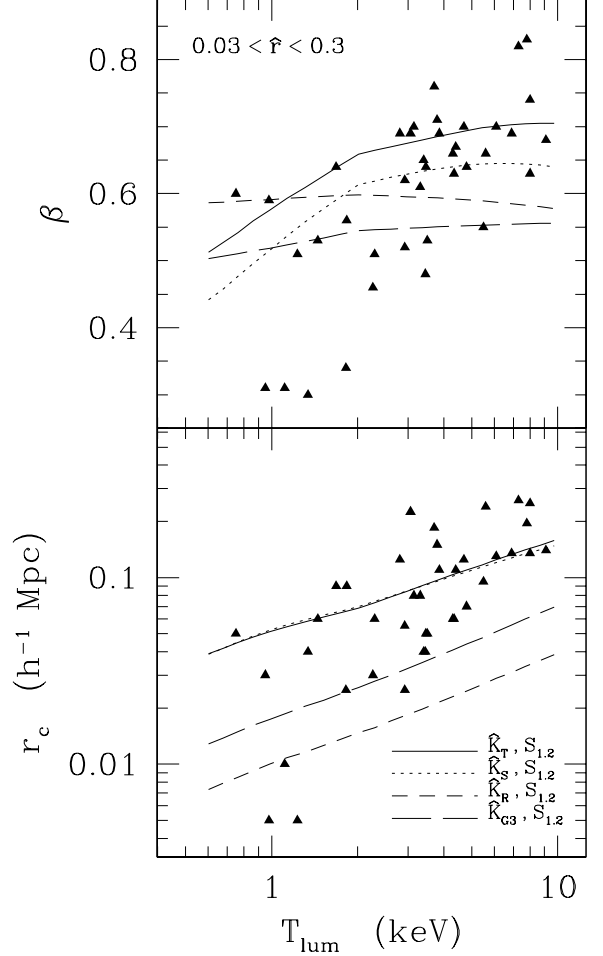


FIG. 18.— Best-fitting β -model parameters to various modified entropy models as a function of luminosity-weighted temperature T_{lum} . As in Figure 17, triangles show measured values of β (upper panel) and r_c (lower panel) compiled by Finoguenov et al. (2001). Solid lines show the values of these parameters in the best fits to truncated modified-entropy models (\hat{K}_T), dotted lines show the best-fitting values for shifted models (\hat{K}_S), short-dashed lines show best fits for radiative-loss model \hat{K}_R , and long-dashed lines show best fits for radiative-loss model \hat{K}_{G3} . All fits were performed over the radial range $0.03 < \hat{r} < 0.3$ for models based on concentration-parameter relation $S_{1,2}$.

The observed dispersion in β and r_c may also depend in part on the amount of gas below the cooling threshold. Figure 18 illustrates how β and r_c depend on the scheme for entropy modification. Shifted models have core radii identical to those of the corresponding truncated models and slightly smaller values of β . However, allowing for radiative losses reduces the best-fitting core radius by a factor of 3–5 and flattens the β - T_{lum} relation, yielding $\beta \approx 0.5$ – 0.6 for fits over the interval $0.03 < r/r_{200} < 0.3$. Other possible sources of dispersion include ellipticity and cluster substructure, which cannot be investigated in the context of our spherically symmetric models.

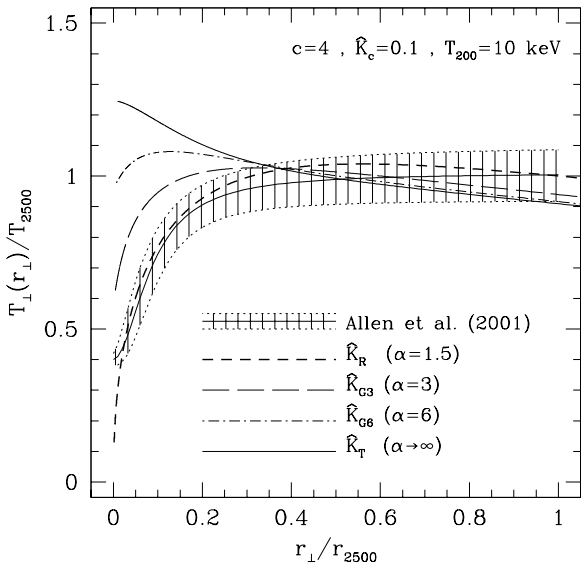


FIG. 19.— Luminosity-weighted projected temperature T_{\perp} as a function of projected radius r_{\perp} . Radii are given in units of the radius r_{2500} within which the mean matter density is 2500 times the critical density. Temperatures are given in units of the mean mass-weighted temperature T_{2500} within r_{2500} . The hatched area shows the best fit of Allen et al. (2001) to their Chandra data on six hot clusters with strong cooling flows, along with the uncertainty in that fit. Other lines show T_{\perp} from modified-entropy models with parameters characteristic of hot clusters: $c = 4$, $\hat{K}_c = 0.1$, and $T_{200} = 10$ keV. The short-dashed line depicts a standard radiative-loss model (\hat{K}_R), the long-dashed line depicts generalized radiative-loss model \hat{K}_{G3} with $\alpha = 3$, the dot-dashed line shows a generalized radiative-loss model with $\alpha = 6$, and the solid line shows a truncated model (\hat{K}_T), in which α is effectively infinite.

3.2.2. Temperature Gradient at Small Radii

The temperature gradient within $\sim 0.3 r_{200}$ also appears to depend on the amount of gas below the cooling threshold. Figure 19, in which the model parameters are appropriate for hot clusters, shows that $T_{\perp}(r_{\perp})$ gradually declines with radius when the entropy distribution is simply truncated at the entropy threshold. Our radiative-loss models, in contrast, have temperatures that rise outward from $r = 0$, then flatten, becoming virtually isothermal out to 30% of the virial radius. As the parameter α drops from the very large values characteristic of truncated models to the canonical radiative-loss value of $3/2$, the region with a positive temperature gradient becomes progressively larger. The run of temperature with radius in our model with $\alpha = 3/2$ is very similar to the “universal” temperature profile observed by Allen et al. (2001) in clusters that appear to have strong cooling flows. In order to facilitate comparison of our models with that data, Figure 19 shows radii in units of r_{2500} , the radius within which the mean matter density is $2500\rho_{cr}$, and temperature in units of T_{2500} , the mean mass-weighted temperature of intracluster gas within r_{2500} . For clusters of this concentration, $r_{2500} \approx 0.3r_{200}$. Note that setting $\alpha = 6$ produces a cluster model with a temperature gradient remaining within 10% of isothermal from small radii to beyond $0.3r_{200}$.

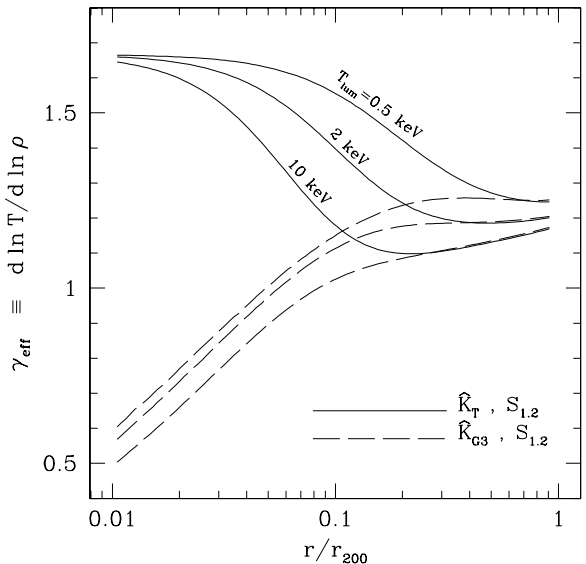


FIG. 20.— Effective polytropic index $\gamma_{\text{eff}} \equiv d \ln P / d \ln \rho$ as a function of radius in modified-entropy models. Solid lines depict truncated models (\hat{K}_T), and dashed lines depict radiative-loss models (\hat{K}_{G3}) with $\alpha = 3$. Results are given for models of clusters with three different luminosity-weighted temperatures ($T_{\text{lum}} = 0.5, 2.0,$ and 10.0 keV, top-to-bottom), using concentration-parameter relation $S_{1.2}$. The curves show that the truncated models are isentropic ($\gamma_{\text{eff}} = 5/3$) at small radii and nearly isothermal ($\gamma_{\text{eff}} \approx 1.1 - 1.2$) at large radii. Values of γ_{eff} in the radiative-loss models are similar at large radii but drop below unity in the radiative-loss models because of the low central temperatures.

3.2.3. Temperature Gradient at Large Radii

Projected cluster temperatures at large radii gradually decline with radius in all of our modified-entropy models. *ASCA* observations of many clusters show evidence for such a decline, which is often expressed as an effective polytropic index $\gamma_{\text{eff}} \equiv d \ln P / d \ln \rho$ (e.g., Markevitch et al. 1998; Markevitch et al. 1999; Ettori & Fabian 1999). These observations indicate that $\gamma_{\text{eff}} \approx 1.2$ outside the cores of clusters. However, recent *XMM-Newton* observations have shown that at least some clusters are nearly isothermal within $0.4 r_{200}$, except for the low-temperature core (Arnaud et al. 2001a,b). The results of § 3.2.2 suggest that radiative losses may be responsible for the isothermal profiles found in these clusters.

Figure 20 shows how γ_{eff} varies with radius in truncated modified-entropy models and in radiative-loss model \hat{K}_{G3} . The cores of the truncated models are nearly isentropic, with $\gamma_{\text{eff}} \approx 5/3$ at $r \lesssim 0.01$. This isentropic region extends to larger radii in cooler halos because their entropy thresholds amount to a larger fraction of the halo’s mean entropy. Outside the isentropic region, we find $\gamma_{\text{eff}} \approx 1.1 - 1.2$, in agreement with observations. The origin of this value of γ_{eff} can be traced back to our assumption that the unmodified gas and dark-matter density profiles are described by identical NFW laws. Komatsu & Seljak (2001) have exploited that same assumption to construct polytropic models for the intracluster medium, finding that $\gamma_{\text{eff}} \approx 1.1 - 1.2$ produces the best agreement between these density profiles at large radii.

The behavior of γ_{eff} in the radiative-loss models is similar to the truncated models at large radii but quite different at small radii. Figure 20 shows that the effective

polytropic index steadily rises from $\gamma_{\text{eff}} < 1$ inside the core through $\gamma_{\text{eff}} \approx 1$ near the core radius to $\gamma_{\text{eff}} \approx 1.1 - 1.2$ at larger radii. The point at which a cluster makes this transition from an isothermal gradient to a mildly declining gradient depends somewhat on cluster temperature. Hot clusters with massive halos tend to have smaller concentrations which allow for near-isothermality at larger radii.

In order to compare our models with observations, we have evaluated γ_{eff} at $r/r_{200} = 0.2$, essentially twice the core radius. This radius is large enough to escape the severe model-dependence of γ_{eff} within the cluster core but small enough that the signal-to-noise in cluster observations still allows for accurate measurements. Figure 21 compares those evaluations of γ_{eff} with the data of Finoguenov et al. (2001). Our models agree with the data, within the large observational uncertainties, and also share the observed (2.5σ) tendency for γ_{eff} to decline with increasing temperature. Two different effects combine to produce higher values of γ_{eff} at low temperature. Because the halos of groups tend to be more concentrated than those of clusters, the scaled temperature T/T_{200} tends to be larger in the cores of groups, leading to higher γ_{eff} . An additional enhancement of γ_{eff} appears in truncated models, in which the entropy threshold has a more significant effect at $0.2r_{200}$ on group scales (see Figure 20).

3.3. Mass-Temperature Relation

Many efforts to measure cosmological parameters such as Ω_M and σ_8 have relied heavily on the cluster mass-temperature relation to link cluster masses to observables like cluster temperature and luminosity (e.g., Henry 1997; Bahcall & Fan 1998; Eke et al. 1998; Donahue & Voit 1999; Borgani et al. 1999; Henry 2000). Until very recently, observers had to rely on M - T relations that were calibrated with numerical simulations (e.g., Evrard et al. 1996; Bryan & Norman 1998). These simulations provide the constant of proportionality \hat{T}_{lum} in the scaling relation

$$T_{\text{lum}} = \hat{T}_{\text{lum}} \frac{(10 \text{ GH})^{2/3} \mu m_p}{2} M_{200}^{2/3}. \quad (21)$$

Values of \hat{T}_{lum} from simulations in the literature can differ by as much as 30%; examples include $\hat{T}_{\text{lum}} \approx 0.9$ from Evrard et al. (1996), $\hat{T}_{\text{lum}} \approx 0.8$ from Bryan & Norman (1998), $\hat{T}_{\text{lum}} \approx 0.9$ from Thomas et al. (2001), and $\hat{T}_{\text{lum}} \approx 0.6$ from the non-radiative simulations of Muanwong et al. (2001). The vast majority of these simulations ignore radiative cooling and supernova heating, both of which can elevate \hat{T}_{lum} . Mass-temperature relations derived from spatially-resolved X-ray observations now suggest that the normalization constant \hat{T}_{lum} derived from simulations is indeed too low (Horner et al. 1999; Nevalainen et al. 2000; Finoguenov et al. 2001). Furthermore, cluster-formation simulations that include radiative cooling also yield a higher normalization constant; for example, $\hat{T}_{\text{lum}} \approx 1.1$ in the radiative simulations of Muanwong et al. (2001).

Our modified-entropy models support these findings. Figure 22 compares two M_{500} - T_{lum} relations derived from our modified-entropy models with the data from Finoguenov et al. (2001) and Nevalainen et al. (2000). In these relations, we scale to M_{500} , the halo mass inside the radius

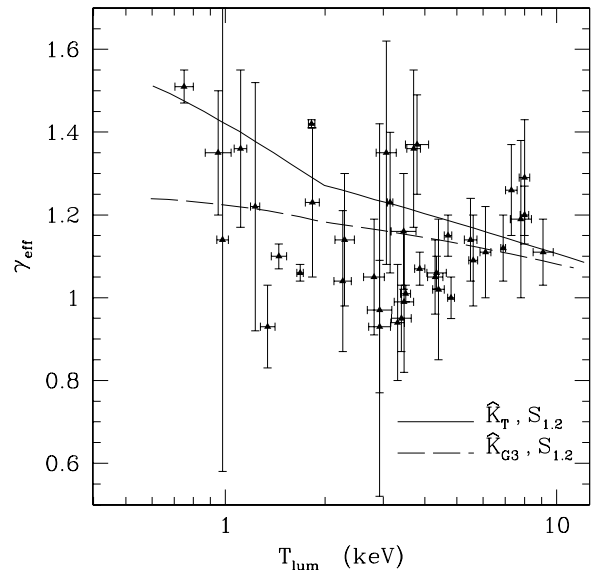


FIG. 21.— Effective polytropic index γ_{eff} as a function of luminosity-weighted temperature T_{lum} . The triangles show γ_{eff} values derived from observed clusters by Finoguenov et al. (2001). The lines show values of γ_{eff} at $r/r_{200} = 0.2$ in truncated modified-entropy models (\hat{K}_T , solid line) and radiative-loss models (\hat{K}_{G3} , dashed line).

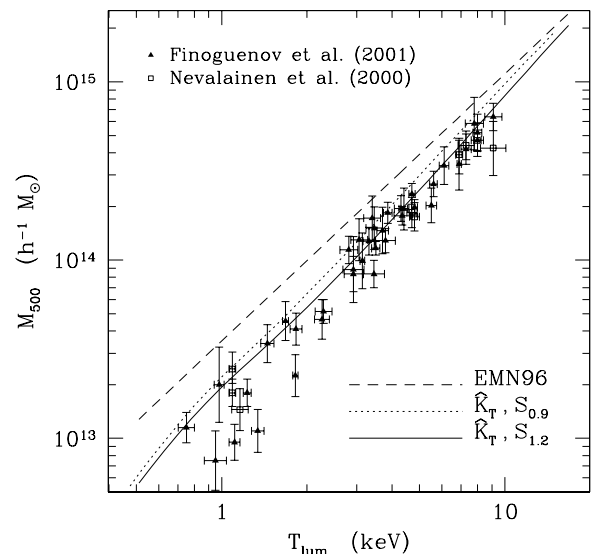


FIG. 22.— Relation between M_{500} and luminosity-weighted temperature (T_{lum}). Solid triangles show mass measurements by Finoguenov et al. (2001), using β -model fitting and the assumption of hydrostatic equilibrium. Open squares show mass measurements by Nevalainen et al. (2000), also using β -model fitting and hydrostatic equilibrium. Both of these data sets were corrected for the presence of cooling flows, so we compare them to our models without radiative losses. The solid and dotted lines show the M_{500} - T_{lum} relations derived from \hat{K}_T models using the concentration parameter relations $S_{1.2}$ and $S_{0.9}$, respectively (see Figure 15). The corresponding relations derived from shifted models (\hat{K}_S) are virtually identical. The dashed line shows the M_{500} - T_{lum} relation derived by Evrard et al. (1996) from simulations that do not include radiative cooling or supernova feedback.

r_{500} within which the mean matter density is $500\rho_{cr}$, because measurements of M_{500} are thought to be more reliable than measurements of M_{200} . The data have been corrected for any cooling flow that might be present in the cluster core, so we compare them to our truncated models with concentration laws $S_{0.9}$ and $S_{1.2}$. The corresponding M_{500} - T_{lum} relations generated from shifted models are virtually identical. Both the truncated and shifted models agree well with the data, but those based on concentration relation $S_{1.2}$ appear to match the data slightly better.

This agreement between the observed M_{500} - T_{lum} relation and the modified-entropy models is quite compelling, considering that the models contain no adjustable parameters. For comparison, Figure 22 also shows the relation derived from simulations by Evrard et al. (1996), which has a lower temperature normalization (equivalent to a higher mass normalization) and a shallower slope. The steeper slope of the M_{500} - T relation from modified-entropy models arises primarily from the dependence of \hat{T}_{lum} on halo concentration. The higher concentration of low-mass halos leads to a higher luminosity-weighted temperature for a given mass. Komatsu & Seljak (2001) find a similar effect in their polytropic cluster models. Entropy modification produces some additional steepening in the relation and shifts its normalization to higher temperatures (see Figure 9).

The greater dispersion and offset toward lower masses at $T_{lum} \approx 1$ seen in Figure 22 could be due to surface-brightness bias (Lloyd-Davies, Bower, & Ponman 2002). Because the gas temperature of intracluster gas in our models tends to decline with radius at large radii, the luminosity-weighted temperature depends on the maximum radius over which that temperature is measured. This effect is negligible in clusters because the bulk of the emission is concentrated around the cluster's core, but it can be significant in groups. Figure 23 shows how the observed M_{500} - T_{lum} relation would depend on the limiting surface-brightness for truncated models with $S_{1.2}$ concentrations. Increasing the surface brightness threshold changes the derived relation in the sense that is observed. Figure 24 shows the relations for different entropy modification schemes at a fixed surface-brightness threshold of $5 \times 10^{-15} \text{ erg cm}^{-2} \text{ s}^{-1} \text{ arcmin}^{-2}$. Truncated and shifted models are affected similarly, but surface-brightness bias has less effect on the radiative-loss model (\hat{K}_{G3}) because its central temperature gradient is closer to isothermal. Some of the scatter to higher temperatures may also arise from the scatter in concentrations expected in low-mass halos (e.g., Afshordi & Cen 2002), but the analysis of Lloyd-Davies et al. (2002) suggests that halo concentration alone cannot account for the large dispersion of the mass-temperature relation for groups.

Despite the excellent agreement between our models and the observations, a word of caution is in order. Both the modified-entropy models and the X-ray mass derivations assume that clusters are in hydrostatic equilibrium. Simulations, on the other hand, suggest the intracluster velocity field is not completely relaxed, with turbulent velocities $\sim 10 - 20\%$ of the sound speed (Ricker & Sarazin 2001). Furthermore, the luminosity-weighted temperature derived from theoretical modeling is not necessarily identical to the spectral-fit temperature derived from obser-

vations (Mathiesen & Evrard 2001). Nevertheless, our results strongly imply that entropy modification and the cosmology-dependent relationship between halo mass and concentration must be accounted for in simulations designed to normalize the cluster mass-temperature relation.

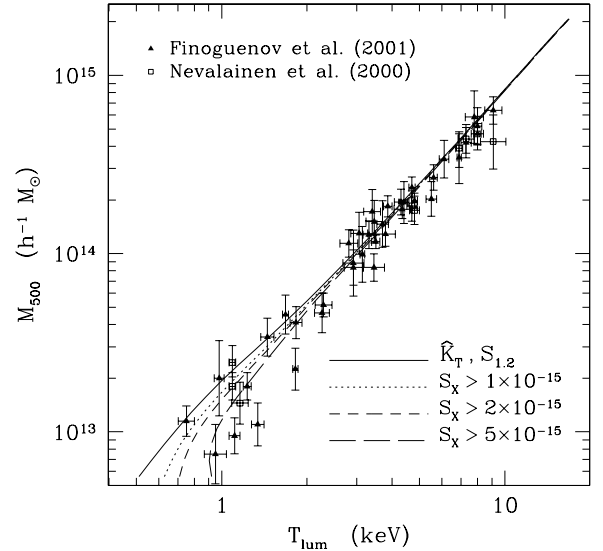


FIG. 23.— Relation between M_{500} and luminosity-weighted temperature (T_{lum}) at different surface-brightness levels. Because temperature declines with radius at large distances from the center of our group models, the limiting surface brightness affects the observed mass-temperature relation. The solid line shows the M_{500} - T_{lum} relation for model $\hat{K}_T, S_{1.2}$. The other lines show how that relation changes when temperature is measured within regions where the bolometric surface brightness in $\text{erg cm}^{-2} \text{ s}^{-1} \text{ arcmin}^{-2}$ exceeds 1×10^{-15} (dotted), 2×10^{-15} (short-dashed), and 5×10^{-15} (long-dashed). The data are the same as in Figure 22. Some of the observed dispersion below the solid line could stem from this surface-brightness bias.

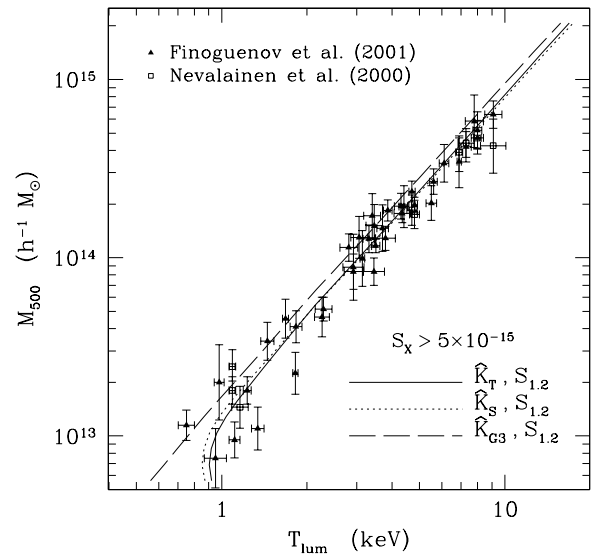


FIG. 24.— Relation between M_{500} and luminosity-weighted temperature (T_{lum}) above a surface brightness of $5 \times 10^{-15} \text{ erg cm}^{-2} \text{ s}^{-1} \text{ arcmin}^{-2}$. The solid and dotted lines show the relation for truncated and shifted models, respectively. The dashed line shows the relation for radiative-loss model \hat{K}_{G3} . The data are the same as in Figure 22. The presence of gas below the cooling threshold near the center of the radiative-loss model lowers the central temperature, thereby mitigating the effects of the surface-brightness threshold.

3.4. Luminosity-Temperature Relation

Our previous work on modified-entropy models and the cooling threshold demonstrated how well these models account for the observed slope and normalization of the cluster luminosity-temperature relation (Voit & Bryan 2001). That paper compared truncated and shifted modified-entropy models to cluster data that were corrected for the effects of cooling flows. Here, we revisit those models and show how the L_X - T_{lum} relation changes when gas below the cooling threshold is included.

Figure 25 shows the L_X - T_{lum} relation for clusters without cooling flows. Of the three models shown, the truncated model with concentration relation $S_{1.2}$ best fits the data, but all three models faithfully describe the L_X - T_{lum} relation equally well on cluster scales. Substituting concentration relation $S_{0.9}$ shifts the models to slightly lower temperatures, but the agreement with groups is almost as good. Using shifted instead of truncated entropy distributions elevates the X-ray luminosity on group scales by a factor ~ 2 .

While there are essentially no free parameters in these models, the cluster luminosity does depend on our assumed value of Ω_M . Raising Ω_M would lower the global ratio of baryons to dark matter, thereby lowering the luminosities of clusters in our models $\propto \Omega_M^{-2}$ (see Eq. 9). Conversely, lowering Ω_M would raise the cluster luminosities. The excellent agreement found here for $\Omega_M = 0.33$ should therefore reinforce confidence in similar measurements of the matter density from the baryon-to-dark-matter ratios of clusters (e.g., Evrard 1997). Our models imply that groups are less suitable for such measurements because their baryon-to-dark-matter ratio within r_{200} may be $\lesssim 50\%$ of the global value (see Figure 3).

The tendency of the data at ~ 1 keV to scatter toward the low- L_X , high- T_{lum} side of the model relations may be due to the same effects that cause similar scatter at those temperatures in the observed M_{500} - T_X relation. Figure 26 shows how surface-brightness bias affects the luminosity-temperature relations derived from our models. Raising the surface-brightness threshold within which luminosity and temperature are measured lowers L_X while raising T_{lum} , producing the same trend seen in the data. Measuring both of these quantities only within regions where $S_X > 5 \times 10^{-15}$ erg cm $^{-2}$ s $^{-1}$ arcmin $^{-2}$ produces relations that track the lower envelope of the group data. Unlike the cluster measurements, the data on groups have not been corrected for the effects of gas below the cooling threshold, which could counterbalance the surface-brightness bias by raising L_X and lowering T_{lum} (see Figure 27). We therefore suspect that the dispersion in the L - T data of Helsdon & Ponman (2000) arises from a combination of differing surface-brightness biases and differing amounts of gas below the cooling threshold.

Reproducing the behavior of clusters and groups with significant amounts of gas below the cooling threshold requires an additional parameter. In our models, that parameter is α , which characterizes the slope of the entropy distribution function below the cooling threshold. Figure 28 shows the relationship between T_{lum} and L_{ROSAT} , the ROSAT-band (0.1-2.4 keV) luminosity, in the data from Markevitch (1998) and in models with differing values of α . Triangles show data corrected to remove the

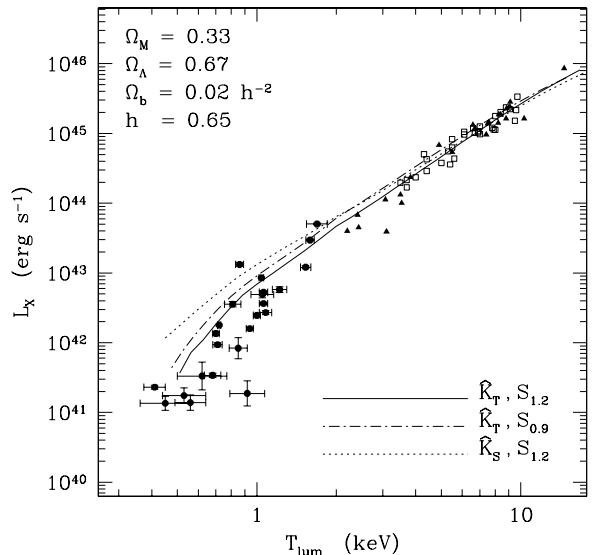


FIG. 25.— Relation between bolometric X-ray luminosity L_X and luminosity-weighted temperature (T_{lum}). Solid triangles show measurements of clusters with insignificant cooling flows compiled by Arnaud & Evrard (1999). Open squares show cooling-flow corrected measurements by Markevitch (1998). Solid circles show group data from Helsdon & Ponman (2000). Because the cluster data are not strongly influenced by cooling flows, we compare them to models without radiative losses. The solid and dotted lines show the L_X - T_{lum} relations derived from truncated (\hat{K}_T) and shifted (\hat{K}_S) models, respectively, and the concentration parameter relation $S_{1.2}$ (see Figure 15). The dot-dashed line shows the relation derived from model \hat{K}_T using the concentration parameter relation $S_{0.9}$. The models assume a standard Λ CDM cosmology with $\Omega_M = 0.33$, $\Omega_\Lambda = 0.67$, and $\Omega_b = 0.02 h^{-2}$, and a Hubble parameter of $h = 0.65$ has been applied to both the models and the data.

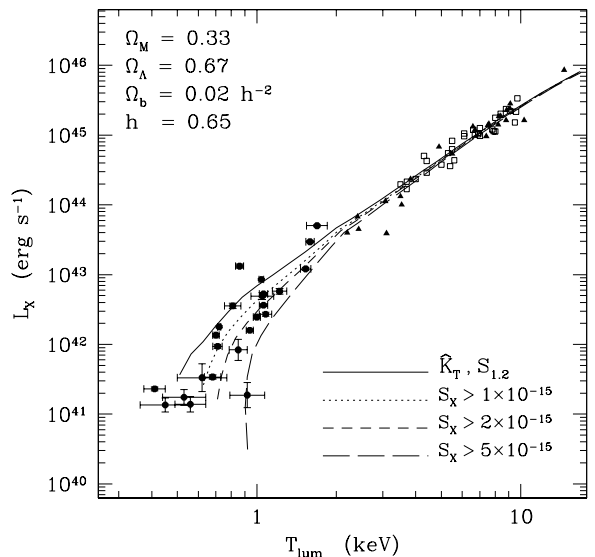


FIG. 26.— Relation between L_X and luminosity-weighted temperature (T_{lum}) at different surface-brightness levels. Because temperature declines with radius at large distances from the center of our group models, the limiting surface brightness affects the observed mass-temperature relation. The solid line shows the L_X - T_{lum} relation for model $\hat{K}_T, S_{1.2}$. The other lines show how that relation changes when temperature and luminosity are measured within regions where the bolometric surface brightness in erg cm $^{-2}$ s $^{-1}$ arcmin $^{-2}$ exceeds 1×10^{-15} (dotted), 2×10^{-15} (short-dashed), and 5×10^{-15} (long-dashed). The data are the same as in Figure 25. Some of the observed dispersion below the solid line could stem from this surface-brightness bias.

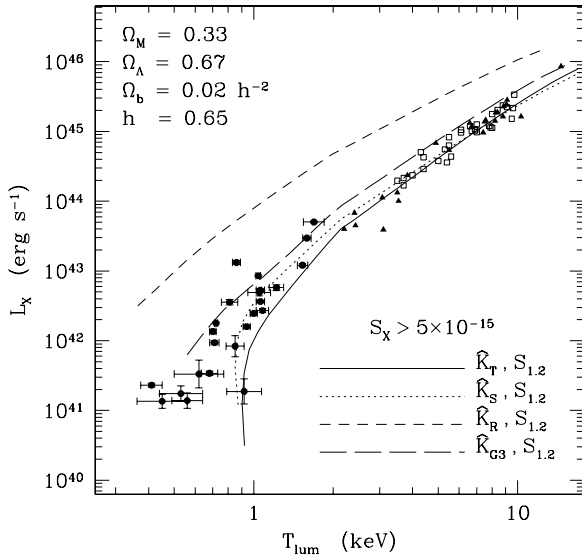


FIG. 27.— Relation between L_X and luminosity-weighted temperature (T_{lum}) above a surface-brightness threshold of $5 \times 10^{-15} \text{ erg cm}^{-2} \text{ s}^{-1} \text{ arcmin}^{-2}$. The solid and dotted lines show the relation for truncated and shifted models, respectively. The short-dashed and long-dashed lines show the relations for radiative-loss models \hat{K}_R and \hat{K}_{G3} , respectively. The data are the same as in Figure 25. The presence of gas below the cooling threshold near the centers of the radiative-loss models lowers the central temperature and raises the central luminosity. Much of the dispersion to the upper left of the solid and dotted lines near $\sim 1 \text{ keV}$ could be due to cooling flows, which have not been corrected for in the group data.

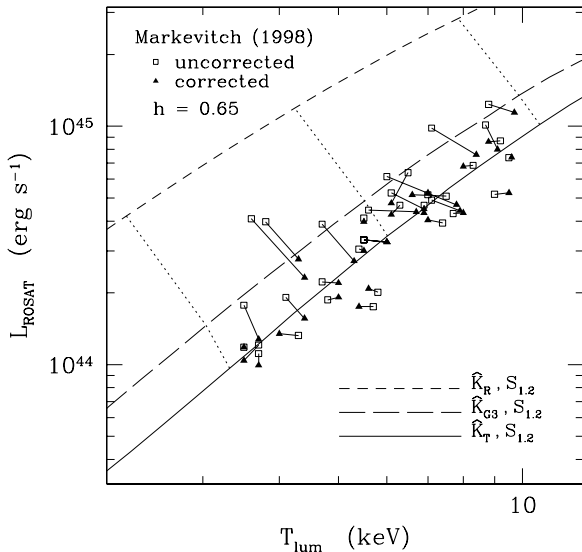


FIG. 28.— Relation between ROSAT (0.1 – 2.4 keV) X-ray luminosity L_{ROSAT} and luminosity-weighted temperature (T_{lum}). Open squares show uncorrected measurements from Markevitch (1998), and solid triangles connected to those squares show results for those same clusters after correcting for a central cooling flow. (Error bars representing temperature uncertainty $\sim 0.5 \text{ keV}$ have been suppressed for legibility.) The solid line shows the $L_{\text{ROSAT}}-T_{\text{lum}}$ relation for truncated models, the long-dashed line depicts model \hat{K}_{G3} ($\alpha = 3$), and the short-dashed line depicts model \hat{K}_R ($\alpha = 3/2$). Dotted lines connect models for identical halo masses, showing how the $L_{\text{ROSAT}}-T_{\text{lum}}$ relation for a given halo mass shifts to higher luminosity and lower temperature as α declines.

effects of gas below the cooling threshold, and the squares connected to those triangles show the uncorrected data. While the corrected data cluster around the line representing truncated models, many of the uncorrected data points lie closer to the line representing radiative-loss models with $\alpha = 3$. A few uncorrected data points stray even farther from the truncated models, toward models with $\alpha < 3$.

Notice that the lines connecting data points with the largest corrections are generally parallel to the lines connecting modified-entropy models with identical halo mass. This agreement suggests that the parameter α adequately characterizes the offset in L_X-T_{lum} space owing to intracluster gas below the cooling threshold. An interesting test of these radiative-loss models would be to compare the value of α inferred from the luminosity-temperature offset to that implied by the inner temperature gradient.

3.5. What governs α ?

The modified-entropy models we have constructed suggest that most of the observable properties of clusters depend on only two parameters. The halo mass M_{200} determines a sort of cluster “main sequence” with well-defined $M_{500}-T_{\text{lum}}$ and L_X-T_{lum} relations. Deviations from those relations and the severity of the inner temperature gradient both depend on a second parameter, α , related to the amount of intracluster gas below the cooling threshold, but what physical processes determine the value of α ?

One is tempted to interpret α in terms of a mass cooling rate \dot{M}_X ; however, *XMM-Newton* observations show little evidence for the low-temperature line emission expected in the standard cooling-flow picture (Peterson et al. 2001). Thus, instead of viewing α as simply a measure of cooling-flow strength, we would like to suggest a wider range of possibilities:

- Entropy history. Our simplistic schemes for entropy modification treat clusters as if they were assembled very early in time, with some standard initial entropy distribution. In fact, the entropy history of the intracluster medium is likely to be far more complex, influenced in differing ways at various times by merger shocks, radiative cooling, and feedback. The dispersion seen in α could stem from differences in the entropy history of clusters, with some evolutionary paths leading to abundant gas below the cooling threshold and other paths leading to very little. If this is the case, then a cluster’s value of α would be an important window into its past.
- Incomplete relaxation. *Chandra* observations of several clusters have revealed “cold fronts” thought to be evidence of low-entropy gas sloshing around in the cores of those clusters (Markevitch et al. 2000; Vikhlinin, Markevitch, & Murray 2001). Our models assume that the lowest-entropy gas in a cluster has already settled into hydrostatic equilibrium at the cluster’s center. Some of the apparent dispersion in α could be due to differences in the degree to which low-entropy gas has settled within cluster cores following the last major merger.

- Recent feedback. Cooling and condensation of low-entropy gas at the center of a cluster is likely to lead to star formation and perhaps enhanced activity in the nucleus of the central galaxy (Fabian 1994). Both star formation and radio jets can provide feedback, imparting entropy to the cluster core that inhibits further condensation (Böhringer et al. 2002). Perhaps these feedback processes control the value of α .
- Thermal conduction. The presence of significant temperature gradients within the cores of some clusters has often been cited as evidence that magnetic fields strongly suppress electron thermal conduction in clusters (Fabian 1994). Recent *Chandra* observations of some particularly sharp cold fronts have reinforced that supposition (Ettori & Fabian 2000). However, these observations constrain conduction in only one dimension and do not necessarily rule out conduction in the other two dimensions. Furthermore, recent theoretical work suggests that magnetic fields might not suppress conduction as effectively as previously believed (Malyskin & Kulsrud 2001; Malyskin 2001; Narayan & Medvedev 2001). It is possible that the magnetic field geometry in a cluster's core places a lower limit on the value of α .

Investigating all of these possibilities is beyond the scope of this paper, but in the next section we explore how one might self-consistently calculate the intracluster entropy distribution within a hierarchical merging scenario.

4. COUPLING ENTROPY, EVOLUTION, AND FEEDBACK

We have shown that some very simple prescriptions for the entropy distribution in present-day clusters lead to a remarkably realistic set of cluster models. However, the astrophysics that leads to these entropy distributions is certainly more complicated than we have assumed. Understanding how the physics of structure formation, cooling, and feedback determine the intracluster entropy distribution will require a more complete theory based on hierarchical merging. This section outlines a few of the basic issues involved in constructing such a theory.

4.1. Entropy Histories

Considering the entropy history of a single gas parcel affords some insight into how radiative cooling establishes an entropy threshold (Voit & Bryan 2001). Suppose that the parcel begins with entropy K_1 in a halo of temperature T_1 at some early time t_1 . In a hierarchical merging scenario, the parcel's halo will eventually merge with another halo at time t_2 . Merger shocks will then raise the parcel's entropy to some new value K_2 , and as that parcel settles within the new halo, it will approach a new temperature T_2 , similar to the characteristic temperature of that new halo. Each subsequent merger will also raise the parcel's temperature and entropy. Thus, the trajectory of a parcel through the entropy-temperature plane can be schematically represented by a sequence of points like that in Figure 29.

The dashed lines in Figure 29 show how the entropy threshold associated with cooling rises with time until

it achieves its present value, indicated by the solid line. As long as a parcel's trajectory through the entropy-temperature plane remains above the cooling threshold, then radiative cooling and subsequent feedback will not significantly affect that parcel's entropy. However, any parcel that spends a large fraction of time below that threshold will be subject to substantial entropy loss, condensation, and whatever feedback ensues. Feedback can continue as long as there are gas parcels below the cooling threshold, but once cooling and feedback have eliminated all gas below the cooling threshold, feedback must cease. Thus, the threshold for entropy modification established by both cooling and feedback corresponds to the cooling threshold defined by the Hubble time t_H .

Although cooling sets the threshold for entropy modification, the model we are describing is not a cooling-flow model. Hierarchical structure formation will ensure that mergers disperse the products of condensation throughout the final cluster. Stars and galaxies form out of the lowest-entropy gas long before the cluster itself forms. Hence, much of the low-entropy gas that would eventually find its way into the cluster core in a simulation with no radiative cooling decouples from the intracluster medium before it can participate in a centrally-focused cooling flow. Finally, for reasons we will describe next, a certain amount of feedback is needed to prevent the incipient intracluster medium from overcooling at high redshift.

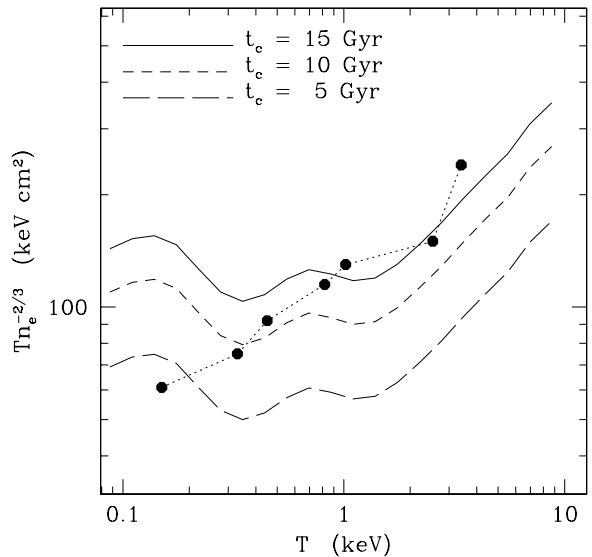


FIG. 29.— Entropy-temperature diagram showing the entropy history of a gas parcel and the evolution of the cooling threshold with time. Solid and dashed lines show the locus in the T - $Tn_e^{-2/3}$ plane at which the cooling time t_c of a gas parcel equals 15 Gyr (solid line), 10 Gyr (short-dashed line) and 5 Gyr (long-dashed line). This locus moves upward through the diagram as the universe ages. The dots connected by dotted lines schematically illustrate the entropy history of a gas parcel as described in the text. As long as the parcel's trajectory through the entropy-temperature plane remains above the cooling threshold, it will not substantially cool. However, both cooling and feedback triggered by that cooling will inevitably modify the entropy of gas parcels that find themselves below the cooling threshold.

4.2. Overcoming Overcooling

Overcooling is one of the classic problems that models of hierarchical structure formation must overcome (Cole 1991; White & Frenk 1991; Blanchard, Valls-Gabaud, & Mamon 1992; Balogh et al. 2001). If radiative cooling were allowed to proceed unchecked as structure formed, then a substantial percentage ($\gtrsim 20\%$) of the universe's baryons would have been locked into condensed objects before the era of cluster formation. Because the fraction of uncondensed baryons in present-day clusters is $\sim 90\%$, feedback processes like supernova heating are presumed to inhibit cooling and condensation of high-redshift baryons (White & Rees 1978; Cole 1991; White & Frenk 1991).

In our models, overcooling manifests itself as an entropy threshold K_c that is much higher than the characteristic entropy of an unmodified high-redshift halo. To illustrate this effect, let us assume that the progenitor halo of a present-day cluster has a temperature $T(z)$ that depends on redshift. The entropy threshold for that halo is then $K_c(z) \propto \{T^{1/2}(z) \Lambda[T(z)] t_H(z)\}^{2/3}$, and the characteristic entropy within r_{200} in the unmodified halo is $K_{200}(z) \propto T(z)H^{-4/3}$. The ratio of these two quantities in the high-redshift limit is thus

$$\frac{K_c}{K_{200}} \propto \left\{ \frac{\Lambda[T(z)]}{T(z)} \right\}^{2/3} [H(z)t_H(z)]^{2/3} H^{2/3}(z). \quad (22)$$

Because $H(z)$ rises and $T(z)$ declines with increasing redshift, this ratio must exceed unity at early times.

We can use extended Press-Schechter theory (Bond et al. 1991; Bower 1991) to approximate $T(z)$ and estimate the temperature, entropy, and redshift scales at which overcooling is problematic. First, to demonstrate the principle with simple scaling relations, we consider a Λ CDM ($\Omega_M = 1$) universe with a power spectrum given by an $n = -2$ power law. In that case, the characteristic mass scale evolves like $M \propto (1+z)^{-6}$, and assuming that $M \propto T^{3/2}(1+z)^{-3/2}$ yields $T(z) \propto (1+z)^{-3}$. At low redshifts, where T is high, we have $\Lambda \propto T^{1/2}$ and $K_c/K_{200} \propto (1+z)^2$. However, at high redshifts, when the progenitor temperature is smaller, we have $\Lambda \propto T^{-1/2}$ and $K_c/K_{200} \propto (1+z)^4$. Thus, the progenitor of a halo with $K_c/K_{200} \approx 0.1$ at $z \approx 0$ would have $K_c/K_{200} \sim 1$ at $z \sim 1-2$.

Figure 30 illustrates this effect more precisely for a Λ CDM universe seeded by a power spectrum with shape parameter $\Gamma = 0.17$. The dashed line shows $K_{200}(z)$ for a halo that reaches $T = 5$ keV at $z = 0$. The solid line shows the entropy threshold K_c in that evolving halo for a metallicity of one-third solar. Feedback must impart an entropy ~ 30 keV cm² to prevent overcooling at $z \gtrsim 3$.

4.3. Interplay between Feedback and Merging

Feedback can solve the overcooling problem, but it introduces another, more subtle problem into our framework. Our modified-entropy models assume that gas above the cooling threshold follows the unmodified distribution $K_0(M_g)$. However, the need for feedback at early times implies that a large proportion of intracluster gas has experienced entropy modification at least once in its history. Somehow, the process of cluster formation needs to restore the unmodified distribution to gas above the threshold at $z = 0$.

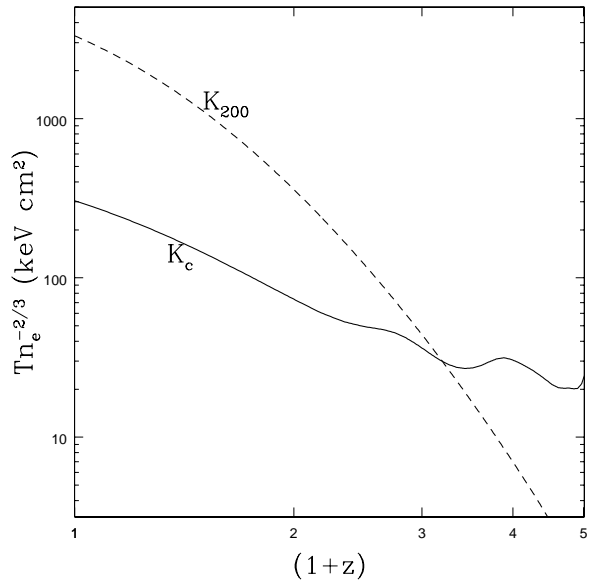


FIG. 30.— Entropy evolution with redshift. The dashed line shows how the characteristic entropy K_{200} of the progenitor halo of a 5 keV cluster at $z = 0$ evolves with redshift in a Λ CDM universe with shape parameter $\Gamma = 0.17$. The solid line shows how the cooling threshold K_c associated with that halo depends on redshift. Because K_{200} falls below the cooling threshold at $z \gtrsim 3$, feedback is needed to prevent the majority of the baryons associated with the progenitor from condensing and forming stars.

Exactly how that happens is unclear. Consider what happens in a merger between two halos containing isothermal gas at temperatures T_1 and T_2 that collide at velocity v . Merger shocks with Mach number $\mathcal{M}_i \propto vT_i^{-1/2}$ will propagate through each halo's gas, raising the entropy of that gas by some more-or-less uniform factor depending on \mathcal{M}_i . This mechanism could potentially amplify the effects of early feedback, which must raise the intrahalo entropy to at least K_c to avoid overcooling. Subsequent shocks would then boost the entropy even further, along a path parallel to the dashed line in Figure 30. If this mechanism dominates, then very little gas should remain near K_c at $z \sim 0$.

However, early feedback is likely to diminish the effects of mergers, particularly in gas with low entropy. If feedback raises all the gas in the progenitor halo of a cluster to $\sim K_c$, then the intrahalo medium will be nearly isentropic, with high-temperature gas at the center of the halo and lower-temperature gas at the outskirts (see Figure 8). When mergers occur, Mach numbers associated with lower-entropy gas in the halo's core will therefore be lower than those associated with higher-entropy gas near the virial radius. Hence, merger shocks will act to steepen any entropy gradient that exists. Dynamical friction may also add to this effect, because the cores of merging halos tend to lose orbital energy before they collide and merge. Another effect to consider is the quasi-continuous accretion of gas associated with small halos, for which the Mach number is likely to be quite high. This type of accretion will enhance the amount of high-entropy gas in the final cluster. Thus, it seems possible that the modified-entropy models we have developed can successfully be linked with hierarchical structure formation, although many details remain to be worked out.

4.4. Excess Energy

Several recent analyses of similarity breaking in groups and clusters have cast the problem in terms of energy rather than entropy (e.g., Wu et al. 1998, 2000; Lloyd-Davies, Ponman, & Cannon 2000; Loewenstein 2000; Bower et al. 2001; Lloyd-Davies et al. 2002). For example, if one knows what the configuration of the intracluster gas would be in the absence of non-gravitational heating and cooling processes, then one can opt to define the “excess energy” of a cluster’s gas to be the difference in total energy between that unmodified configuration and the actual configuration. Depending on what is assumed about the unmodified configuration, these excess energies can range from $\sim 0.3 - 1.0$ keV for groups (e.g., Lloyd-Davies et al. 2000, 2002) to over 2 keV for clusters (e.g., Wu et al. 2000).

The results of this paper indicate that some combination of heating and cooling is responsible for similarity breaking because cooling is needed to explain the core entropies of clusters and groups and heating is needed to prevent overcooling at early times. Therefore, we prefer to compute excess energy in a way that explicitly accounts for the separate contributions of cooling and heating. First, we assume that the baseline state of a cluster of mass M_{200} is a truncated model from which cooling and condensation has removed a fraction f_* of the lowest-entropy gas. In other words, the initial configuration of the intracluster medium has an entropy floor equal to $K_0(f_*)$ and contains a fraction $1 - f_*$ of the cluster’s baryons. Then, we assume that the final state of the cluster is a shifted model with the same proportion of baryons but an entropy floor equal to the cooling threshold, so that it obeys the observed M - T and L - T relations. Formally, the entropy distribution of the final state is $K(f_g) = K_0(f_g) + K_c(T_{\text{lum}})$ with an outer boundary where $f_g = 1 - f_*$. Because the amount of hot baryonic gas in both models is the same, the amount of heat input required to explain the cluster scaling relations after a fraction f_* of the intracluster gas has condensed equals the energy input needed to convert the initial configuration to the final configuration, including work done at the outer boundary of the intracluster medium.

Figure 31 shows the energy difference between these configurations as a function of halo mass for different values of the condensed baryon fraction f_* . To facilitate comparisons with other treatments of excess energy, we divide this energy difference by the total number of particles in an unmodified cluster ($f_b M_{200} / \mu m_p$), giving the quantity $\Delta\epsilon$ in units of keV per particle. When the condensed baryon fraction is small ($f_* = 0.02$), the excess energy needed to account for the scaling relations of massive clusters ($\sim 10^{15} M_\odot$) approaches the ~ 3 keV level. However, this large amount of excess energy depends heavily on the assumed form of the unmodified entropy distribution, which is likely to be a poor approximation for these purposes. The large difference in the excess energy of massive clusters between models with $f_* = 0.02$ and $f_* > 0.05$ indicates that a large amount of energy is needed to lift the lowest-entropy gas out of the very center of the gravitational potential. Yet, Figure 1 shows that the unmodified intracluster density distribution is unlikely to be as centrally condensed as we have assumed. Even in the absence

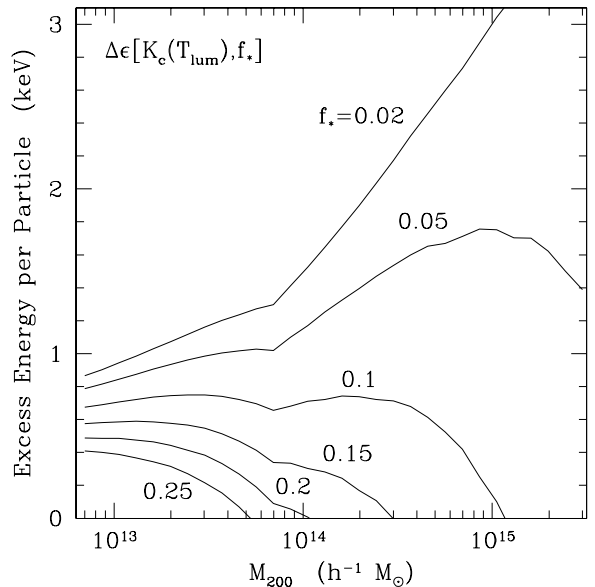


FIG. 31.— Excess energy required to overcome the cooling threshold for different values of the condensed baryon fraction (f_*). At each halo mass M_{200} , the quantity $\Delta\epsilon[K_c(T_{\text{lum}}), f_*]$ is the energy input per particle needed to transform the truncated entropy distribution $\hat{K}_T(f_*)$, from which a fraction f_* of the lowest-entropy baryons have been removed, into a shifted distribution $\hat{K}_S = \hat{K}_0 + \hat{K}_c$ containing the remaining fraction $1 - f_*$ of the baryons. This transformation corresponds to first removing gas without adding heat energy, then adding enough heat to reproduce the L - T and M - T relations. The energy input required to produce these relations for plausible condensed-baryon fractions of $f_* \approx 0.1 - 0.2$ is $\sim 0.4 - 0.7$ keV particle $^{-1}$ at group scales and is negligible for hot clusters.

of cooling, the true unmodified profile probably corresponds more closely to a truncated model with $\hat{K}_c \sim 0.05 - 0.1$, which substantially reduces the excess energy burden. Thus, when calculating excess energies for clusters, one must make sure that the baseline model accurately represents the cluster configuration in the absence of heating.

The curve with $f_* = 0.1$ is likely to be a more realistic representation of the heat input needed to explain the scaling properties of massive clusters for two reasons: (1) this value of f_* roughly corresponds to the fraction of cluster baryons that have condensed into stars, and (2) when $f_* \gtrsim 0.1$, truncation eliminates the innermost part of the entropy distribution that is discrepant with simulations. At $10^{15} M_\odot$, this excess energy curve suggests that only a fraction of a keV per particle is needed to explain cluster scaling relations. That is because a shifted model with an entropy shift determined by the cooling threshold is virtually identical to a truncated model with the innermost f_* of gas removed. Likewise, the mass scales at which curves with larger values of f_* intercept the zero-energy level also indicate cases in which the truncated and shifted models are virtually identical, requiring no excess heating to produce the observed scaling relations. In the limiting case of zero supernova heating (e.g., Bryan 2000, Muanwong et al. 2001), these intercept points show the fraction of condensed baryons implied by the L - T relation as a function of halo mass.

If the condensed baryon fractions of groups are similar to those of clusters, then $\sim 0.3 - 0.7$ keV of excess energy is needed to explain the M - T and L - T relations at ~ 1 keV.

The main difference between the initial configuration and the final configuration of groups with $f_* \sim 0.1 - 0.25$ is that the gas in the final configuration is considerably more extended, with substantially more gravitational potential energy. Because models with higher f_* contain less intragroup gas, they are less extended, and less energy is needed to change their configuration. We note that the excess energy needs of groups are comparable to estimates of the supernova energy released over the course of the group’s history (e.g., Ponman et al. 1999, Loewenstein 2000; Pipino et al. 2002), which may mean that no other source of energy is needed to explain their scaling properties, if that energy efficiently heats the intragroup medium.

The bottom line here is that calculations of the heat input needed to account for the scaling relations of clusters and groups depend critically on what is assumed to happen in the absence of heat input. Most calculations of excess energy have assumed that the intracluster gas density obeys either a simple polytropic equation of state (e.g., Wu et al. 2000; Loewenstein 2000) or a β -model density profile (e.g., Bower et al. 2001; Lloyd-Davies et al. 2002) whose parameters are adjusted according to the amount of heat input. The modified-entropy models discussed in this paper allow for cooling and condensation of the lowest-entropy gas to occur before heat is added. Figure 31 demonstrates that the amount of heating needed to explain the scaling relations depends strongly on the amount of cooling that occurs prior to heat input and that realistic amounts of “precooling” substantially reduce the required amount of non-gravitational heating.

5. CONCLUSIONS

A realistic family of models for clusters in hydrostatic and convective equilibrium can be constructed using the Navarro, Frenk, & White (1997) density profile and some rudimentary prescriptions for how radiative cooling and feedback induced by that cooling modify the entropy distribution of intracluster gas. The models presume that the intracluster entropy distribution in the absence of cooling and feedback would be identical to that of gas that takes on the same density distribution as the dark matter as it settles into the cluster’s potential well—an assumption supported by numerical simulations. Because the lowest-entropy gas within that distribution can cool within a Hubble time, its entropy must somehow be modified. The threshold entropy in our prescriptions for entropy modification corresponds to the entropy at which the cooling time of intracluster gas equals the age of the universe. The prescriptions themselves include truncation of the entropy distribution at the threshold entropy, shifting of the entropy distribution by adding the threshold entropy to the entire distribution, and a qualitative implementation of radiative cooling.

Exploring the properties of dimensionless models depending only on the halo concentration c , the dimensionless entropy threshold \hat{K}_c , and the prescription for entropy modification reveals that:

- Removal of low-entropy gas acts to flatten the core density profile, regardless of whether cooling or heating eliminates that low-entropy gas (see Figures 1 and 4).

- The observable properties of clusters depend more critically on the threshold entropy than on the mode of entropy modification. For example, truncation of the intracluster entropy distribution at a given value of \hat{K}_c and shifting of the entropy distribution by that same amount lead to very similar pressure, density, and temperature profiles within the cluster’s virial radius (see Figures 4 and 8).
- Within about 30% of the virial radius, the surface-brightness profiles of truncated and shifted models are very similar to β -models (see Figure 5). Raising the entropy threshold tends to lower the best-fitting value of β , while raising the halo concentration tends to decrease the core radius (see Figures 6 and 7).
- All of our prescriptions for entropy modification tend to augment the luminosity-weighted temperature of a cluster as the entropy threshold rises. However, that temperature increase is relatively small because the increased central entropy decreases the luminosity of high-temperature gas in the core. Thus, modifying the entropy of a cluster shifts the bulk of a cluster’s luminosity to larger radii, where gas temperatures tend to be smaller, mitigating the effects of the entropy increase (see § 2.5).
- All of our prescriptions for entropy modification reduce the X-ray luminosity of a cluster as the entropy threshold rises. In the high-threshold limit, dimensionless luminosity scales as $\hat{L} \propto \hat{K}_c^{-3/2}$, owing to the asymptotic $\rho \propto r^{-3}$ scaling of the unmodified NFW density distribution at large radius (see § 2.6). When luminosity scales with the entropy threshold in this way, the L - T relation should not flatten below ~ 2 keV, where line cooling dominates free-free emission, and the relation should also evolve little with time. The observed L - T relation shares both of these features. Furthermore, this scaling of luminosity with the entropy threshold leads to an L - T relation slightly steeper than $L \propto T_{\text{lum}}^{5/2}$, with the extra steepening coming from the tendency for low-temperature halos to be more concentrated, also in agreement with observations.

Adopting relations between halo concentration c and halo mass M_{200} that are drawn from simulations and supported by observations enables us to generate models for real clusters that reproduce many of their observable properties:

- Fitting β -models to our modified-entropy clusters yields β and core-radius values that are similar to those of observed clusters. Our models reproduce the observed tendency for β to be lower in low-temperature halos, a behavior that arises because the entropy threshold determined by cooling has a much larger impact on low-temperature halos. Our models also reproduce the observed relationship

between core radius and temperature, implying that $r_c \approx 0.1 r_{200}$, regardless of temperature. Despite the flattening of the density profile in low-temperature halos, the core radius remains near $0.1 r_{200}$ because of the increased halo concentration (see Figures 6 and 7). The large dispersion observed in β and r_c could arise from a number of effects, some involving observational systematics such as surface-brightness bias and the range of radii in the fit, others involving physical differences such as cluster-to-cluster variations in the amount of gas below the cooling threshold (see Figures 17 and 18).

- The temperature gradient at small radii in our model clusters depends sensitively on the amount of gas below the cooling threshold, closely related to the parameter α in our radiative-loss models. In our most extreme radiative-loss model, with $\alpha = 3/2$, the temperature gradient at $\lesssim 0.3 r_{200}$ is very similar to the “universal” temperature gradient observed by Allen et al. (2001). As the parameter α rises to infinity, the limit in which no gas lies below the cooling threshold, the inner temperature gradient flattens and then reverses, monotonically decreasing with radius in the large α limit (see Figure 19).
- All of our models have a negative temperature gradient at large radii because the underlying potential is steeper than isothermal at those radii. In order to compare our models with observations, we compute the effective polytropic index $\gamma_{\text{eff}} \equiv d \ln P / d \ln \rho$ as a function of radius. At the virial radius, we find $\gamma_{\text{eff}} \approx 1.1 - 1.2$, but the behavior of γ_{eff} at smaller radii depends strongly on the nature of entropy modification. In models with no gas below the cooling threshold, the cluster core is nearly isentropic, with $\gamma_{\text{eff}} \approx 5/3$. In models with significant amounts of gas below that threshold, we find $\gamma_{\text{eff}} \lesssim 1$ within the core radius, a consequence of the positive temperature gradient (see Figure 20). Values of γ_{eff} evaluated at $0.2 r_{200}$ agree with observations, within the large observational uncertainties (see Figure 21).
- The mass-temperature relations derived from our truncated and shifted modified-entropy models, which have no gas below the cooling threshold, agree well with those derived from cluster observations that have been corrected for the presence of cooling flows (see Figure 22). The slope of this relation is steeper than the $M \propto T^{3/2}$ expectation from self-similar scaling because low-temperature halos are more concentrated, leading to a slightly higher temperature for a given mass (see Figure 9), a feature these models share with those of Komatsu & Seljak (2001). Clusters of a given temperature are less massive than those in simulations without cooling and feedback because entropy modification owing to these processes shifts all of our model clusters to higher temperature. However, the agreement between

observations and our models does not necessarily imply that this M - T relation is without problems, as both the observational determinations and the models assume that the intracluster medium is an ideal gas in hydrostatic equilibrium, which may not be the case. Furthermore, this relation does not apply to clusters that have not been corrected for cooling flows—the temperature normalization at a given mass in our radiative-loss models can be up to 30% lower, depending on the value of α (see Figures 11 and 12).

- The luminosity-temperature relations derived from truncated and shifted models also agree well with those derived from cooling-flow corrected observations of clusters (see Figure 25). While there are no adjustable parameters in these models, the baryon-to-dark-matter ratio does depend on our assumed value of $\Omega_M = 0.33$. Thus, this agreement can be taken as additional evidence for a low value of Ω_M .
- Gas below the cooling threshold both raises the X-ray luminosity and lowers the luminosity-weighted temperature of our model clusters. Hence, the L - T relations derived from our radiative-loss models lie above and to the left of the truncated and shifted models in the L - T plane. Changing α leads to a displacement almost perpendicular to the L - T relations themselves (see Figure 28). Correcting for cooling-flow emission leads to a very similar displacement in L - T space, suggesting that the L - T relation for uncorrected clusters may depend almost entirely on the two parameters M_{200} and α . It will be interesting to see whether values of α derived from displacement in L - T space agree with those implied by the inner temperature gradient.

The modified-entropy models we have derived can account for many of the observed properties of present-day clusters, but they are obviously too simplistic to tell us how those clusters got to be the way they are. Somehow, hierarchical structure formation generated intracluster entropy distributions similar to our simple prescriptions for entropy modification. Cooling, feedback, and merging all have important roles to play. The consistency of our models with the data strongly suggests that radiative cooling sets the level of the intracluster entropy threshold and substantially reduces the amount of heat input needed to explain the observed scaling relations. However, radiative cooling unchecked by feedback would lead to overcooling of intrahalo gas at $z \sim 2 - 3$ (see § 4.2). At least some feedback is needed to keep $\sim 90\%$ of intergalactic baryons in gaseous form, as observed. Mergers following an episode of feedback can potentially amplify the entropy generated by that feedback, when low-density gas associated with low-temperature halos is shocked. However, the overall impact of mergers on intracluster entropy remains unclear. Determining just how cooling, mergers, and feedback conspire to produce the present-day entropy distribution of clusters will require high-resolution numerical simulations and semi-analytical modeling focusing on the intergalactic entropy distribution and how it evolves.

We acknowledge Megan Donahue and Don Horner for helpful conversations and Trevor Ponman and Stefano Borgani for comments on the original manuscript. MLB

is supported by a PPARC rolling grant for extragalactic astronomy and cosmology at the University of Durham.

REFERENCES

- Afshordi, N., & Cen, R. 2002, *ApJ*, 564, 669
 Allen, S. W., Schmidt, R. W., & Fabian, A. C., 2001, *MNRAS*, 328, 37
 Arnaud, M. et al. 2001a, *A&A*, 365, L67
 Arnaud, M., Neumann, D. M., Aghanim, N., Gastaud, R., Majerowicz, S., & Hughes, J. P. 2001b, *A&A*, 365, 80
 Arnaud, M., & Evrard, A. E. 1999, *MNRAS*, 305, 631
 Babul, A., Balogh, M. L., Lewis, G. F., & Poole, G. B. 2002, *MNRAS*, 330, 329
 Bahcall, N. A., & Fan, X. 1998, *ApJ*, 504, 1
 Balogh, M. L., Babul, A., & Patton, D. R. 1999, *MNRAS*, 307, 463
 Balogh, M. L., Pearce, F. R., Bower, R. G., & Kay, S. T. 2001, *MNRAS*, 326, 1228
 Bardeen, J. M., Bond, J. R., Kaiser, N., & Szalay, A. S. 1986, *ApJ*, 304, 15
 Bialek, J. J., Evrard, A. E., & Mohr, J. J. 2001, *ApJ*, 555, 597
 Blanchard, A., Valls-Gabaud, D., & Mamon, G. A. 1992, *A&A*, 264, 365
 Böhringer, H., Matsushita, K., Churazov, E., Ikebe, Y., & Chen 2002, *A&A*, 382, 804
 Bond, J. R., Cole, S., Efstathiou, G., & Kaiser, N. 1991, *ApJ*, 379, 440
 Borgani, S., Governato, F., Wadsley, J., Menci, N., Tozzi, P., Lake, G., Quinn, T., & Stadel, J. 2001a, *ApJ*, 559, L71
 Borgani, S., Rosati, P., Tozzi, P., & Norman, C. 1999, *ApJ*, 517, 40
 Borgani, S., Rosati, P., Tozzi, P., Stanford, S. A., Eisenhardt, P. R., Lidman, C., Holden, B., Della Ceca, R., Norman, C., & Squires, G. 2001b, *ApJ*, 561, 13
 Bower, R. G. 1991, *MNRAS*, 248, 332
 Bower, R. G. 1997, *MNRAS*, 288, 355
 Bower, R. G., Benson, A. J., Lacey, C. G., Baugh, C. M., Cole, S., & Frenk, C. S. 2001, *MNRAS*, 325, 497
 Bryan, G. L. 1999, *Computing in Science & Engineering*, 1999, 1, 46
 Bryan, G. L. 2000, *ApJ*, 544, L1
 Bryan, G. L., & Norman, M. L. 1998, *ApJ*, 495, 80
 Bryan, G. L., & Voit, G. M. 2001, *ApJ*, 556, 590
 Cavaliere, A., & Fusco-Femiano, R. 1978, *A&A*, 70, 677
 Cavaliere, A., Menci, N., & Tozzi, P. 1999, *MNRAS*, 308, 599
 Cole, S. 1991, *ApJ*, 367, 45
 da Silva, A. C., Kay, S. T., Liddle, A. R., Thomas, P. A., Pearce, F. R., & Borbosa, D. 2001, *ApJ*, 561, 15
 Della Ceca, R., Scaramella, R., Gioia, I. M., Rosati, P., Fiore, F., & Squires, G. 2000, *A&A*, 353, 498
 Donahue, M. E., & Voit, G. M. 1999, *ApJ*, 523, 137L
 Donahue, M. E., Voit, G. M., Scharf, C. A., Gioia, I. M., Mullis, C. R., Hughes, J. P., & Stocke, J. T. 1999, *ApJ*, 527, 525
 Edge, A. C., & Stewart, G. C. 1991, *MNRAS*, 252, 414
 Eke, V. R., Cole, S., & Frenk, C. S. 1996, *MNRAS*, 282, 263
 Eke, V. R., Cole, S., Frenk, C. S., & Henry, J. P. 1998, *MNRAS*, 298, 1145
 Eke, V., Navarro, J. F., & Frenk, C. S. 1998, *ApJ*, 503, 569
 Eke, V., Navarro, J. F., & Steinmetz, M. 2001, *ApJ*, 554, 114
 Ettori, S., & Fabian, A. C. 1999, *MNRAS*, 305, 834
 Ettori, S., & Fabian, A. C. 2000, *MNRAS*, 317, L57
 Evrard, A. E. 1997, *MNRAS*, 292, 289
 Evrard, A. E., & Henry, J. P. 1991, *ApJ*, 383, 95
 Evrard, A. E., Metzler, C., & Navarro, J. F. 1996, *ApJ*, 469, 494
 Fabian, A. C. 1994, *ARA&A*, 32, 277
 Frenk et al. 1999, *ApJ*, 525, 554
 Finoguenov, A., Reiprich, T. H., & Böhringer, H. 2001, *A&A*, 368, 749
 Helsdon, S. F., & Ponman, T. J. 2000, *MNRAS*, 315, 356
 Henry, J. P. 1997, *ApJ*, 4898, 1L
 Henry, J. P. 2000, *ApJ*, 534, 565
 Henry, J. P., & Arnaud, K. A. 1991, *ApJ*, 372, 410
 Heinz, S., Reynolds, C. R., & Begelman, M. C. 1998, *ApJ*, 501, 126
 Horner, D. J., Mushotzky, R. F., & Scharf, C. A. 1999, *ApJ*, 520, 78
 Kaiser, C. R., & Alexander, P. 1999, *MNRAS*, 305, 707
 Kaiser, N. 1986, *MNRAS*, 222, 323
 Kaiser, N. 1991, *ApJ*, 383, 104
 Kitayama, T., & Suto, Y. 1997, *ApJ*, 490, 557
 Knight, P. A., & Ponman, T. J. 1997, *MNRAS*, 289, 955
 Komatsu, E., & Seljak, U. 2001, *MNRAS*, 327, 1353
 Lewis, G. F., Babul, A., Katz, N., Quinn, T., Hernquist, L., & Weinberg, D. H. 2000, *ApJ*, 536, 623
 Lloyd-Davies, E. J., Bower, R. G., & Ponman, T. J. 2002, *astro-ph/0203502*
 Lloyd-Davies, E. J., Ponman, T. J., & Cannon, D. B. 2000, *MNRAS*, 315, 689
 Loewenstein, M. 2000, 532, 17
 Malyshkin, L. 2001, *ApJ*, 554, 561
 Malyshkin, L., & Kulsrud, R. 2001, *ApJ*, 549, 402
 Markevitch, M. 1998, *ApJ*, 504, 27
 Markevitch, M. et al. 2000, *ApJ*, 541, 542
 Markevitch, M., Forman, W. R., Sarazin, C. L., & Vikhlinin, A. 1998, *ApJ*, 503, 77
 Markevitch, M., Vikhlinin, A., Forman, W. R., & Sarazin, C. L. 1999, *ApJ*, 503, 77
 Mathiesen, B. F., & Evrard, A. E. 2001, *ApJ*, 546, 100
 Metzler, C., & Evrard, A. E. 1994, *ApJ*, 437, 564
 Metzler, C., & Evrard, A. E. 1997, *astro-ph/9710324*
 Muanwong, O., Thomas, P. A., Kay, S. T., Pearce, F. R., & Couchman, H. M. P. 2001, *ApJ*, 552, 27L
 Narayan, R., & Medvedev, M. V. 2001, *ApJ*, 562, L129
 Navarro, J. F., Frenk, C. S., & White, S. D. M. 1995, *MNRAS*, 275, 720
 Navarro, J. F., Frenk, C. S., & White, S. D. M. 1997, *ApJ*, 490, 493
 Nevalainen, J., Markevitch, M., & Forman, W. 2000, *ApJ*, 532, 694
 Norman, M. L., & Bryan, G. L. 1998, *Numerical Astrophysics 1998*, ed. S. Miyama & K. Tomisaka, (Dordrecht: Kluwer), p. 19
 Oukbir, J., & Blanchard, A. 1997, *A&A*, 317, 1
 Pearce, F., Thomas, P. A., Couchman, H. M. P., & Edge, A. C. 2000, *MNRAS*, 319, 209
 Peterson, J. R. et al. 2001, *A&A*, 365, L104
 Pipino, A., Matteucci, F., Borgani, S., & Biviano, A. 2000, *New Astronomy*, in press, *astro-ph/0204161*
 Ponman, T. J., Cannon, D. B., & Navarro, J. F. 1999, *Nature*, 397, 135
 Raymond, J. C., & Smith, B. W. 1997, *ApJS*, 35, 419
 Reiprich, T. H., & Böhringer, H. 2001, *astro-ph/0111285*
 Reynolds, C. R., Heinz, S., & Begelman, M. C. 2002, *astro-ph/0201271*
 Ricker, P. M., & Sarazin, C. L. 2001, *ApJ*, 561, 621
 Sugihara, T., & Ostriker, J. P. 1998, *ApJ*, 507, 16
 Sugiyama, N. 1995, *ApJS*, 100, 281
 Thomas, P. A., Muanwong, O., Kay, S. T., & Liddle, A. R. 2001a, *astro-ph/0112449*
 Thomas, P. A., Muanwong, O., Pearce, F. R., Couchman, H. M. P., Edge, A. C., Jenkins, A., & Onuora, L. 2001b, *MNRAS*, 324, 450
 Tozzi, P., & Norman, C. 2001, *ApJ*, 546, 63
 Valageas, P., & Silk, J. 1999, *A&A*, 350, 725
 Van Waerbeke, L. et al. 2001, *A&A*, 374, 757
 Viana, P. T. P., & Liddle, A. R. 1996, *MNRAS*, 281, 323
 Viana, P. T. P., Nichol, R. C., & Liddle, A. R. 2001, *astro-ph/0111394*
 Vikhlinin, A., Forman, W., Jones, C. 1999, *ApJ*, 525, 47
 Vikhlinin, A., Markevitch, M., Murray, S. S. 2001, *ApJ*, 551, 160
 Voit, G. M. 2000, *ApJ*, 543, 113
 Voit, G. M., & Bryan, G. L. 2001, *Nature*, 414, 425
 White, S. D. M., Efstathiou, G., & Frenk, C. S. 1993, *MNRAS*, 262, 1023
 White, S. D. M., & Frenk, C. S. 1991, *MNRAS*, 379, 52
 White, S. D. M., & Rees, M. 1978, *MNRAS*, 183, 341
 Wu, K. K. S., Fabian, A. C., & Nulsen, P. E. J. 1998, *MNRAS*, 20, 301L
 Wu, K. K. S., Fabian, A. C., & Nulsen, P. E. J. 2000, *MNRAS*, 318, 889
 Wu, X.-P., & Xue, Y.-J. 2002, *ApJ*, in press, (*astro-ph/0112274*)
 Xu, H., Jin, G., & Wu, X.-P. 2001 *ApJ*, 553, 78